

Dalitz plot analysis of the $D^+ \rightarrow \pi^- \pi^+ \pi^+$ decay

G. Bonvicini,¹ D. Cinabro,¹ M. Dubrovin,¹ A. Lincoln,¹ D. M. Asner,² K. W. Edwards,² P. Naik,² R. A. Briere,³ T. Ferguson,³ G. Tatishvili,³ H. Vogel,³ M. E. Watkins,³ J. L. Rosner,⁴ N. E. Adam,⁵ J. P. Alexander,⁵ D. G. Cassel,⁵ J. E. Duboscq,⁵ R. Ehrlich,⁵ L. Fields,⁵ R. S. Galik,⁵ L. Gibbons,⁵ R. Gray,⁵ S. W. Gray,⁵ D. L. Hartill,⁵ B. K. Heltsley,⁵ D. Hertz,⁵ C. D. Jones,⁵ J. Kandaswamy,⁵ D. L. Kreinick,⁵ V. E. Kuznetsov,⁵ H. Mahlke-Krüger,⁵ D. Mohapatra,⁵ P. U. E. Onyisi,⁵ J. R. Patterson,⁵ D. Peterson,⁵ J. Pivarski,⁵ D. Riley,⁵ A. Ryd,⁵ A. J. Sadoff,⁵ H. Schwarthoff,⁵ X. Shi,⁵ S. Stroiney,⁵ W. M. Sun,⁵ T. Wilksen,⁵ S. B. Athar,⁶ R. Patel,⁶ J. Yelton,⁶ P. Rubin,⁷ C. Cawfield,⁸ B. I. Eisenstein,⁸ I. Karliner,⁸ D. Kim,⁸ N. Lowrey,⁸ M. Selen,⁸ E. J. White,⁸ J. Wiss,⁸ R. E. Mitchell,⁹ M. R. Shepherd,⁹ D. Besson,¹⁰ T. K. Pedlar,¹¹ D. Cronin-Hennessy,¹² K. Y. Gao,¹² J. Hietala,¹² Y. Kubota,¹² T. Klein,¹² B. W. Lang,¹² R. Poling,¹² A. W. Scott,¹² A. Smith,¹² P. Zweber,¹² S. Dobbs,¹³ Z. Metreveli,¹³ K. K. Seth,¹³ A. Tomaradze,¹³ J. Ernst,¹⁴ K. M. Ecklund,¹⁵ H. Severini,¹⁶ W. Love,¹⁷ V. Savinov,¹⁷ O. Aquines,¹⁸ A. Lopez,¹⁸ S. Mehrabyan,¹⁸ H. Mendez,¹⁸ J. Ramirez,¹⁸ G. S. Huang,¹⁹ D. H. Miller,¹⁹ V. Pavlunin,¹⁹ B. Sanghi,¹⁹ I. P. J. Shipsey,¹⁹ B. Xin,¹⁹ G. S. Adams,²⁰ M. Anderson,²⁰ J. P. Cummings,²⁰ I. Danko,²⁰ D. Hu,²⁰ B. Moziak,²⁰ J. Napolitano,²⁰ Q. He,²¹ J. Insler,²¹ H. Muramatsu,²¹ C. S. Park,²¹ E. H. Thorndike,²¹ F. Yang,²¹ M. Artuso,²² S. Blusk,²² J. Butt,²² N. Horwitz,²² S. Khalil,²² J. Li,²² N. Mena,²² R. Mountain,²² S. Nisar,²² K. Randrianarivony,²² R. Sia,²² T. Skwarnicki,²² S. Stone,²² and J. C. Wang²²

(CLEO Collaboration)

¹Wayne State University, Detroit, Michigan 48202

²Carleton University, Ottawa, Ontario, Canada K1S 5B6

³Carnegie Mellon University, Pittsburgh, Pennsylvania 15213

⁴Enrico Fermi Institute, University of Chicago, Chicago, Illinois 60637

⁵Cornell University, Ithaca, New York 14853

⁶University of Florida, Gainesville, Florida 32611

⁷George Mason University, Fairfax, Virginia 22030

⁸University of Illinois, Urbana-Champaign, Illinois 61801

⁹Indiana University, Bloomington, Indiana 47405

¹⁰University of Kansas, Lawrence, Kansas 66045

¹¹Luther College, Decorah, Iowa 52101

¹²University of Minnesota, Minneapolis, Minnesota 55455

¹³Northwestern University, Evanston, Illinois 60208

¹⁴State University of New York at Albany, Albany, New York 12222

¹⁵State University of New York at Buffalo, Buffalo, New York 14260

¹⁶University of Oklahoma, Norman, Oklahoma 73019

¹⁷University of Pittsburgh, Pittsburgh, Pennsylvania 15260

¹⁸University of Puerto Rico, Mayaguez, Puerto Rico 00681

¹⁹Purdue University, West Lafayette, Indiana 47907

²⁰Rensselaer Polytechnic Institute, Troy, New York 12180

²¹University of Rochester, Rochester, New York 14627

²²Syracuse University, Syracuse, New York 13244

(Dated: July 2, 2007)

Abstract

Using 281 pb⁻¹ of data recorded by the CLEO-c detector in e^+e^- collisions at the $\psi(3770)$, corresponding to 0.78 million D^+D^- pairs, we investigate the substructure of the decay $D^+ \rightarrow \pi^-\pi^+\pi^+$ using the Dalitz plot technique. We find that our data are consistent with the following intermediate states: $\rho(770)\pi^+$, $f_2(1270)\pi^+$, $f_0(1370)\pi^+$, $f_0(1500)\pi^+$, $f_0(980)\pi^+$, and $\sigma\pi^+$. We confirm large S wave contributions at low $\pi\pi$ mass. We set upper limits on contributions of other possible intermediate states. We consider three models of the $\pi\pi$ S wave and find that all of them adequately describe our data.

I. INTRODUCTION

The study of charmed meson hadronic decays illuminates light meson spectroscopy. Many of these decays proceed via quasi two-body modes and are subsequently observed as three or more stable particles. In this work our goal is to describe the two-body resonances that contribute to the observed three-body $D^+ \rightarrow \pi^-\pi^+\pi^+$ decay. Study of a given state can shed light on different production mechanisms.

We present here a study of charged D decay to three charged pions carried out with the CLEO detector. This mode has been studied previously by E687 [1], E691 [2], E791 [3], and FOCUS [4]. The analyses from E791 and FOCUS have roughly the same data size as the one described here, while the E687 and E691 analyses used about an order of magnitude smaller samples and are not discussed further.

E791 uses the isobar technique, where each resonant contribution to the Dalitz plot [5] is modeled as a Breit-Wigner amplitude with a complex phase. This works well for narrow, well separated resonances, but when the resonances are wide and start to overlap, solutions become ambiguous, and unitarity is violated. In contrast, FOCUS uses the K-matrix approach, which gives a description of S wave $\pi\pi$ resonances treating the σ (also known as $f_0(600)$) and $f_0(980)$ contributions in a unified way. While this approach is a step forward, some authors [6], [7] have claimed that the exact formalism used by FOCUS violates chiral constraints, and might therefore lead to unphysical behavior at low $\pi\pi$ mass, where the S wave is most prominent. Despite the difference in approach the two techniques give a good description of the observed Dalitz plots and agree about the overall contributions of the resonances, as is shown in Table I. Both experiments see that about half of the fit fraction for this decay is explained by a low $\pi^+\pi^-$ mass S wave. We have in hand a comparable sample of $D^+ \rightarrow \pi^-\pi^+\pi^+$ decays (inclusion of the charge-conjugate mode is always implicit); we can thus check this somewhat surprising result in a significantly different environment.

E791 and FOCUS are fixed target experiments where D mesons are produced within a momentum range of 10-100 GeV/ c . In our experiment D^+ mesons are produced in the process $e^+e^- \rightarrow \psi(3770) \rightarrow D^+D^-$, close to the threshold, and are thus almost at rest. This difference of production environments is important for observation of events from the decay $D^+ \rightarrow K_S^0\pi^+$, which has a large rate and contributes to the same final state. These events are easily removed in the fixed target experiments by requiring all three charged pions to be consistent with a common vertex, and its residual contribution was estimated to be small. We are forced to take a different approach as the lower momentum K_S^0 does not produce clearly detached vertexes when $K_S^0 \rightarrow \pi^+\pi^-$. Nevertheless we are able to clearly isolate the $K_S^0\pi^+$ channel, using the $\pi^+\pi^-$ invariant mass.

Our analysis compares several different models for this decay, attempting to find the best description. One is an isobar model where we have included the best description of the σ from Ref. [6] and the Flatté parameterization for the threshold effects on the $f_0(980)$ [8]. We use two other S wave models, both of which satisfy chiral constraints and respect unitarity. A model by Schechter and his collaborators (Schechter model) [9] is based on the linear sigma model of the chiral symmetric Lagrangian. It includes only the lowest lying $\pi\pi$ S wave resonances, the σ and the $f_0(980)$. A model by Achasov and his collaborators (Achasov model) [10] is field-theory based and has been developed to describe scattering experiments. We compare the results of these three models of the resonance contributions to the Dalitz plot to see if one description is superior to the others and to understand differences among the models.

TABLE I: A comparison of the observed fit fractions in % from previous studies of $D^+ \rightarrow \pi^- \pi^+ \pi^+$. The sum of all fit fractions is not necessarily equal to 100% due to the ignored interference terms. The ‘‘S wave π^+ ’’ entry for E791 is the sum of the three entries above it.

Mode	E791 [3]	FOCUS [4]
$\sigma\pi^+$	46.3 ± 9.2	
$f_0(980)\pi^+$	6.2 ± 1.4	
$f_0(1370)\pi^+$	2.3 ± 1.7	
S wave π^+	54.8 ± 9.5	56.0 ± 3.9
$\rho^0(770)\pi^+$	33.6 ± 3.9	30.8 ± 3.9
$f_2(1270)\pi^+$	19.4 ± 2.5	11.7 ± 1.9

In Section II we briefly describe the CLEO-c experiment and the basic algorithms of event reconstruction. In Section III we describe the event selection for the Dalitz plot analysis. The formalism of fitting the observed Dalitz plot, and systematic cross-checks are given in Section IV. Appendix VII describes in detail the two $\pi^+\pi^-$ S wave models that we use, some of which are extensions of published theoretical work. We summarize our results in Section V.

II. DETECTOR AND EXPERIMENTAL TECHNIQUE

CLEO-c is a general purpose detector which includes a tracking system for measuring momenta and specific ionization of charged particles, a Ring Imaging Cherenkov detector to aid particle identification, and a CsI calorimeter for detection of electromagnetic showers. These components are immersed in a magnetic field of 1 T, provided by a superconducting solenoid, and surrounded by a muon detector. The CLEO-c detector is described in detail elsewhere [11].

This analysis utilizes 281 pb⁻¹ of data collected on the $\psi(3770)$ resonance at $\sqrt{s} \simeq 3773$ MeV at the Cornell Electron Storage Ring, corresponding to production of about 0.78×10^6 D^+D^- pairs. We reconstruct the $D^+ \rightarrow \pi^- \pi^+ \pi^+$ decay using three tracks measured in the tracking system. Charged tracks satisfy standard goodness of fit quality requirements [12]. Pion candidates are required to have specific ionization, dE/dx , in the main drift chamber within four standard deviations of the expected value for a pion at the measured momentum. Tracks coming from the origin must have an impact parameter with respect to the beam spot (in the plane transverse to the beam direction) of less than 5 mm. We do not reconstruct the $K_S^0 \rightarrow \pi^+\pi^-$ vertex, but the requirement on pion track impact parameter removes $\sim 60\%$ of events with $K_S^0 \rightarrow \pi^+\pi^-$ decays. The remaining events from $D^+ \rightarrow K_S^0 \pi^+$ represent about one third of those selected for the Dalitz plot.

III. EVENT SELECTION

Selection of events from the $D^+ \rightarrow \pi^- \pi^+ \pi^+$ decay is done with two signal variables:

$$\Delta E = E_D - E_{\text{beam}}, \quad (1)$$

$$m_{\text{BC}} = \sqrt{E_{\text{beam}}^2 - p_D^2}, \quad (2)$$

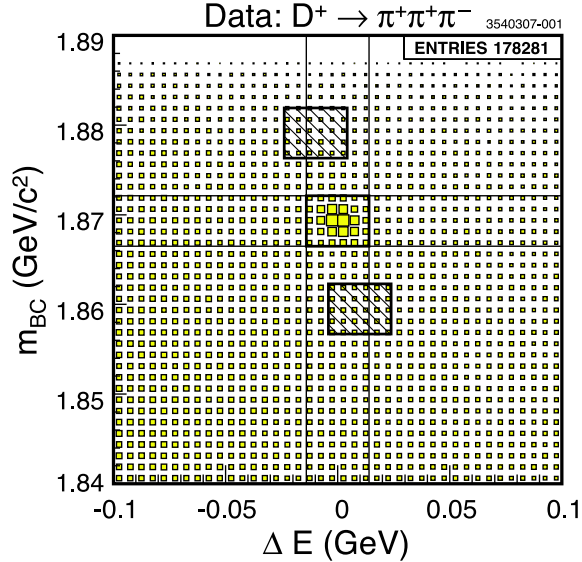


FIG. 1: The m_{BC} vs. ΔE distribution of events passing all selection requirements described in the text. The center box shows the signal region for the Dalitz plot analysis. The two hatched boxes show the sidebands. The vertical and horizontal lines restrict the regions of events plotted in Figs. 2 and 3, respectively.

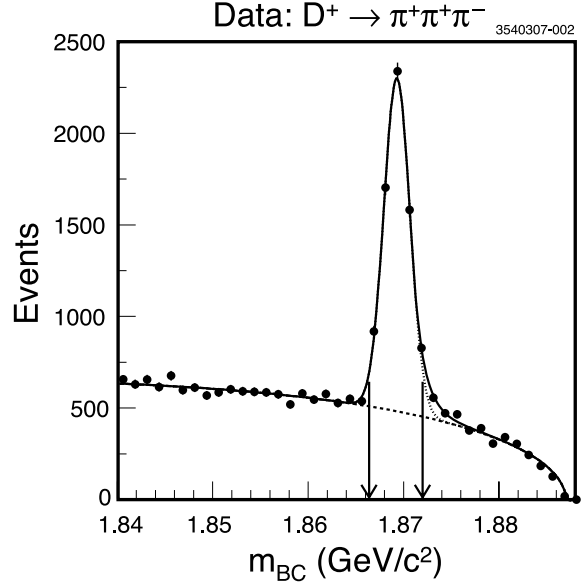


FIG. 2: The m_{BC} distribution of events from the $|\Delta E| < 2\sigma(\Delta E)$ range. Dashed curve shows a contribution from the background, dotted curve is a Gaussian part of the Crystal Ball function for the signal shape, and solid curve is total, signal plus background. Events between arrows are selected for the Dalitz plot analysis.

where E_{beam} is a beam energy, and E_D and p_D are the energy and momentum of the reconstructed D meson candidate, respectively. The beam crossing angle of ~ 4 mrad is used to calculate the D meson candidate energy and momentum in the $\psi(3770)$ center of mass system. We require $|\Delta E| < 2\sigma(\Delta E)$, $|m_{\text{BC}} - m_D| < 2\sigma(m_{\text{BC}})$, where resolutions $\sigma(\Delta E) = 5.5 \pm 0.4$ MeV and $\sigma(m_{\text{BC}}) = 1.38 \pm 0.03$ MeV/ c^2 represent the widths of the signal peak in the 2D-distribution shown in Fig. 1, and the projections, Fig. 2 and Fig. 3. To determine the efficiency we use a GEANT-based Monte Carlo simulation where one of the charged D meson decays in a signal mode uniformly in phase space, while the other decays to all known modes with relevant branching fractions. Simulated events are required to pass the same selection requirements as data. The shape of the background contribution in the Dalitz analysis is estimated using events from the two hatched side-band boxes shown in Fig. 1. The sideband boxes are shifted in ΔE to select the background events whose $\pi^-\pi^+\pi^+$ invariant mass range is consistent with the signal box.

This selection gives 6991 events in the signal box. From a fit to the m_{BC} distribution, shown in Fig. 2, we find 2159 ± 18 of these to be background. The $K_S^0 \rightarrow \pi^+\pi^-$ contribution to the sample of events in the signal box is easily seen as a sharp peak in the invariant $\pi^+\pi^-$ mass spectrum shown in Fig. 4. The K_S^0 contribution is well described by a Gaussian shape with resolution $\sigma(m_{\pi^+\pi^-}) = 3.5$ MeV/ c^2 both in data and the simulation. The number of events in the K_S^0 peak is 2239 ± 77 from a fit to a Gaussian signal plus linear background. Excluding $K_S^0\pi^+$ fraction and the background leaves ~ 2600 signal events of the $D^+ \rightarrow \pi^-\pi^+\pi^+$ decay. From these yields we calculate branching fractions, $\mathcal{B}(D^+ \rightarrow \pi^-\pi^+\pi^+) =$

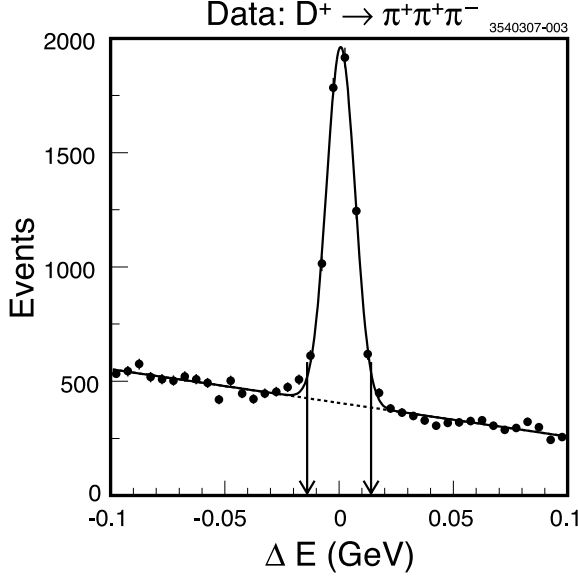


FIG. 3: The ΔE distribution of events from the $|m_{BC} - m_D| < 2\sigma(m_{BC})$ range. Events between the arrows are selected for the Dalitz plot.

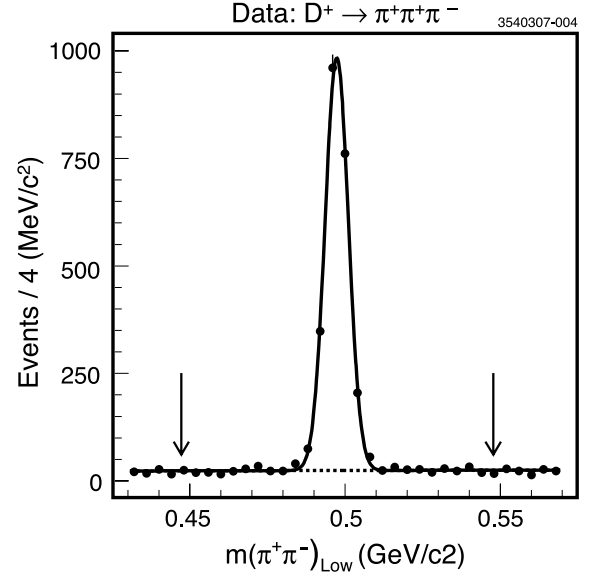


FIG. 4: The $m(\pi^+\pi^-)_{\text{Low}}$ distribution of events pre-selected for the Dalitz plot. A clear signal for the $K_S^0 \rightarrow \pi^+\pi^-$ decay is observed. Events in the range between the arrows, $0.2 < m^2(\pi^+\pi^-)_{\text{Low}} < 0.3 \text{ (GeV/c}^2\text{)}^2$, are discarded from the Dalitz plot analysis.

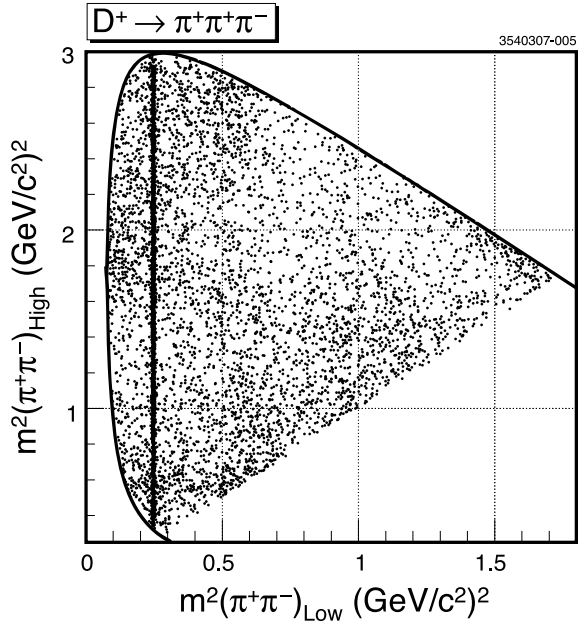


FIG. 5: The Dalitz plot for $D^+ \rightarrow \pi^-\pi^+\pi^+$ candidates.

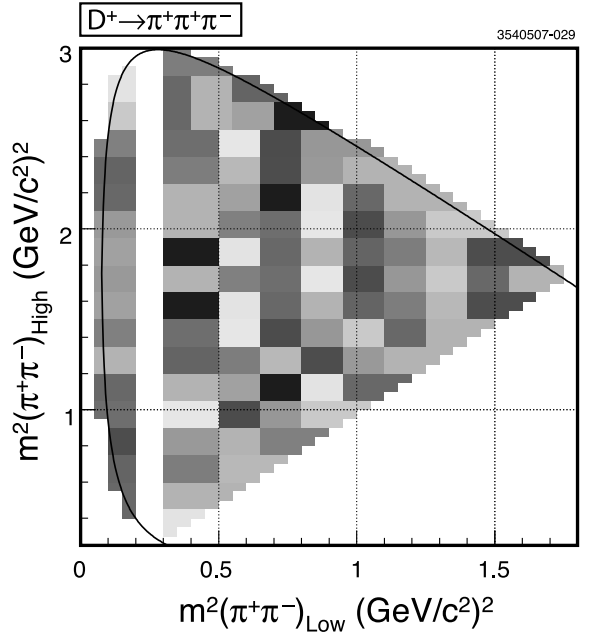


FIG. 6: The adaptive binning scheme.

$(0.33 \pm 0.01)\%$ and $\mathcal{B}(D^+ \rightarrow K_S^0 \pi^+) = (1.59 \pm 0.06)\%$ (statistical errors are shown only), which are consistent with recently published CLEO-c results $\mathcal{B}(D^+ \rightarrow \pi^- \pi^+ \pi^+) = (0.34 \pm 0.02)\%$ [13] and $\mathcal{B}(D^+ \rightarrow K_S^0 \pi^+) = (1.55 \pm 0.05 \pm 0.06)\%$ [12]. This cross-check demonstrates the quality of our simulation and validity of assumptions about the background level.

The presence of two π^+ mesons impose a Bose-symmetry of the $\pi^- \pi^+ \pi^+$ final state. The Bose-symmetry when interchanging the two same sign charged pions is explicitly accounted for in our amplitude parameterization. We analyze events on the Dalitz plot by choosing $x \equiv m^2(\pi^+ \pi^-)_{\text{Low}}$ and $y \equiv m^2(\pi^+ \pi^-)_{\text{High}}$ as the independent (x, y) variables. The third variable $z \equiv m^2(\pi^+ \pi^+)$ is dependent on x and y through the energy-momentum balance equation. This choice folds all the data into the top half of the kinematically allowed region, as is shown in Fig. 5. The contribution from $D^+ \rightarrow K_S^0 \pi^+$ is clearly seen as the narrow vertical band with $m(\pi^+ \pi^-)_{\text{Low}} \simeq m_{K_S^0}$. In our Dalitz plot analysis we do not consider events in the band $0.2 < m^2(\pi^+ \pi^-)_{\text{Low}} < 0.3$ $(\text{GeV}/c^2)^2$, which is approximately ten times our $K_S^0 \rightarrow \pi^+ \pi^-$ mass resolution. This leaves 4086 (signal and background) events for our Dalitz plot analysis.

IV. DALITZ PLOT ANALYSIS

A. Formalism

This Dalitz plot analysis exploits the techniques and formalism described in Ref. [14] that have been applied in many other CLEO analyses. We use an unbinned maximum likelihood fit that minimizes the sum over N events:

$$\mathcal{L} = -2 \sum_{n=1}^N \log \mathcal{P}(x_n, y_n), \quad (3)$$

where $\mathcal{P}(x, y)$ is the probability density function (p.d.f.), depends on the event sample to be fit,

$$\mathcal{P}(x, y) = \begin{cases} \varepsilon(x, y) & \text{for efficiency;} \\ B(x, y) & \text{for background;} \\ f_{\text{sig}} \mathcal{N}_S |\mathcal{M}(x, y)|^2 \varepsilon(x, y) + (1 - f_{\text{sig}}) \mathcal{N}_B B(x, y) & \text{for signal.} \end{cases} \quad (4)$$

The shapes for the efficiency, $\varepsilon(x, y)$, and background, $B(x, y)$, are explicitly $x - y$ symmetric, third order polynomial functions. To account for efficiency loss in the corners of the Dalitz plot, due to low momentum tracks that are not reconstructed, we use three multiplicative threshold functions that drop the efficiency to zero when one of the Dalitz variables x , y , or z is at their maximum values. The background shape parameterization also includes the non-coherent addition of three resonances $\rho(770)$, $f_2(1270)$, and K_S^0 . The signal p.d.f. is proportional to the efficiency-corrected matrix element squared, $|\mathcal{M}(x, y)|^2$, whose fraction is f_{sig} . We estimate $f_{\text{sig}} = 0.548 \pm 0.013$ from the fit to the m_{BC} mass spectrum after removing events of the K_S^0 contribution. The background term has a relative $(1 - f_{\text{sig}})$ fraction. The signal and the background fractions are normalized separately, $1/\mathcal{N}_S = \int |\mathcal{M}(x, y)|^2 \varepsilon(x, y) dx dy$, $1/\mathcal{N}_B = \int B(x, y) dx dy$, which provides the overall p.d.f. normalization, $\int \mathcal{P}(x, y) dx dy = 1$. The matrix element is a sum of partial amplitudes,

$$\mathcal{M} = \sum_R c_R A_R \Omega_R F_R, \quad (5)$$

where A_R is a mass and spin-dependent function, Ω_R is an angular distribution [14], and F_R is the Blatt-Weisskopf angular momentum barrier-penetration factor [15]. In our standard fit the complex factor $c_R = a_R e^{i\phi_R}$ is represented by two real numbers, an amplitude a_R and a phase ϕ_R . These are included in the list of fit parameters and can be left to float freely or fixed.

For well established resonances, such as $\rho(770)$, $f_2(1270)$, $f_0(1370)$, $f_0(1500)$, $f_0(1710)$, etc., A_R is modeled with the Breit-Wigner function

$$A_R(m) = \frac{1}{m_R^2 - m^2 - im_R\Gamma_R(m)}, \quad (6)$$

where m is the $\pi^+\pi^-$ invariant mass, m_R and $\Gamma_R(m)$ are the resonance mass and mass dependent width [14], respectively. The A_R parameterization of the $f_0(980)$, whose mass, m_{f_0} , is close to the $K\bar{K}$ production threshold, uses the Flatté [8] formula

$$A_{f_0(980)}(m) = \frac{1}{m_{f_0}^2 - m^2 - i[g_{f_0\pi\pi}^2\rho_{\pi\pi}(m) + g_{f_0K\bar{K}}^2\rho_{K\bar{K}}(m)]}, \quad (7)$$

where $g_{f_0\pi\pi}$ and $g_{f_0K\bar{K}}$ are the $f_0(980)$ coupling constants of the resonance to the $\pi\pi$ and $K\bar{K}$ final states, and $\rho_{ab}(m) = 2p_a/m$ is a phase space factor, calculated for the decay products momentum, p_a , in the resonance rest frame.

We model a low mass $\pi\pi$ S wave, σ or $f_0(600)$, in a number of ways. To compare our results with E791 we try a simple spin-0 Breit-Wigner. We also tested a complex pole amplitude proposed in Ref. [6]:

$$A_\sigma(m) = \frac{1}{m_\sigma^2 - m^2}, \quad (8)$$

where $m_\sigma = (0.47 - i0.22)$ GeV is a pole position in the complex $s = m^2(\pi^+\pi^-)$ plane estimated from the results of several experiments. We also consider two comprehensive parameterizations of the low mass $\pi\pi$ S wave. One of them, suggested by J. Schechter, is discussed in Section IV C, and its formalism is presented in Appendix VII A. Another one, suggested by N.N. Achasov, is discussed in Section IV D, and its formalism is presented in Appendix VII B.

B. Fits with Isobar Model

We begin our Dalitz plot analysis by attempting to reproduce the fit results E791 [3]. Our amplitude normalization and sign conventions are different from E791. We therefore compare the phases and fit fractions only. In Fit#1 the contributions from $\rho(770)\pi^+$, $f_0(980)\pi^+$, $f_2(1270)\pi^+$, $f_0(1370)\pi^+$, $\rho(1450)\pi^+$, and non-resonant intermediate states are included. Fit#1 gives a probability of $\simeq 0$. We checked that the inclusion of a $\sigma\pi$ contribution, Fit #2, agrees better with the data giving a fit probability of $\simeq 20\%$. We obtain good agreement comparing our results with Fit#1 and Fit#2 discussed in Ref. [3]. Then, we systematically study possible contributions from all known $\pi^+\pi^-$ resonances listed in Ref. [16]: $\rho(770)$, $f_2(1270)$, $f_0(1370)$, $\rho(1450)$, $f_0(1500)$, $f_0(1710)$, and $f_0(1790)$. We do not consider $f_2'(1525)$ due to its negligible branching fraction to $\pi^+\pi^-$. We assume that high mass resonances $\rho_3(1690)$ and $\rho(1700)$, having non-uniform angular distributions at the

edge of the kinematically allowed region, are well enough represented by $f_0(1710)$, which is a $K\bar{K}$ dominated resonance. The asymptotic “tails” of other known higher mass resonances, $f_2(1950)$, $f_4(2050)$, are effectively accounted for in our fits by the $f_0(1790)$ contribution. We also include a unitary amplitude parametrization of the $\pi^+\pi^+$ S -wave with isospin $I=2$ from Ref. [17]. For the $f_0(980)$ we use the Flatté formula, Eq. 7, with parameters taken from the recent BES II measurement [18]. For the σ we switch to a complex pole amplitude, Eq. 8, rather than the spin-0 Breit-Wigner used by E791.

Starting from the contributions clearly seen in our fit, which is equivalent to Fit#2 of E791 [3], we add or remove additional resonances one by one in order to improve the consistency between the model and data. We use Pearson’s χ^2 statistic criterion [16] for adaptive bins to calculate the probability of consistency between the p.d.f. and the data on the Dalitz plot. The bins are shown in Fig. 6. We also consider the variation of the log likelihood to judge improvement. We keep a contribution for the next iteration if its amplitude is significant at more than three standard deviations and the phase uncertainty is less than 30° . Table II shows the list of surviving contributions with their fitted amplitudes

TABLE II: Results of the isobar model analysis of the $D^+ \rightarrow \pi^-\pi^+\pi^+$ Dalitz plot. For each contribution the relative amplitude, phase, and fit fraction is given. The errors are statistical and systematic, respectively.

Mode	Amplitude (a.u.)	Phase ($^\circ$)	Fit fraction (%)
$\rho(770)\pi^+$	1(fixed)	0(fixed)	$20.0 \pm 2.3 \pm 0.9$
$f_0(980)\pi^+$	$1.4 \pm 0.2 \pm 0.2$	$12 \pm 10 \pm 5$	$4.1 \pm 0.9 \pm 0.3$
$f_2(1270)\pi^+$	$2.1 \pm 0.2 \pm 0.1$	$-123 \pm 6 \pm 3$	$18.2 \pm 2.6 \pm 0.7$
$f_0(1370)\pi^+$	$1.3 \pm 0.4 \pm 0.2$	$-21 \pm 15 \pm 14$	$2.6 \pm 1.8 \pm 0.6$
$f_0(1500)\pi^+$	$1.1 \pm 0.3 \pm 0.2$	$-44 \pm 13 \pm 16$	$3.4 \pm 1.0 \pm 0.8$
σ pole	$3.7 \pm 0.3 \pm 0.2$	$-3 \pm 4 \pm 2$	$41.8 \pm 1.4 \pm 2.5$

and phases, and calculated fit fractions. The sum of all fit fractions is 90.1%, and the fit probability is $\simeq 28\%$ for 90 degrees of freedom. The best p.d.f. and the two projections of the Dalitz plot and selected fit components are shown in Figs. 7, 8, and 9. For contributions that are not significant we set upper limits at the 95% confidence level, as shown in Table III. The “N.R.” represents a non-resonant contribution which is assumed to populate the Dalitz plot uniformly with a constant phase.

TABLE III: Upper limit on the fit fraction, at the 95% confidence level, for contributions that we do not find significant in the $D^+ \rightarrow \pi^-\pi^+\pi^+$ isobar model Dalitz plot analysis.

Mode	Upper limit on fit fraction (%)
$\rho(1450)\pi^+$	<2.4
N.R.	<3.5
$I=2 \pi^+\pi^+$ S wave	<3.7
$f_0(1710)\pi^+$	<1.6
$f_0(1790)\pi^+$	<2

The systematic uncertainties, shown in Table II, are estimated from numerous fit variations. We study the stability of the nominal fit results by adding or removing degrees of

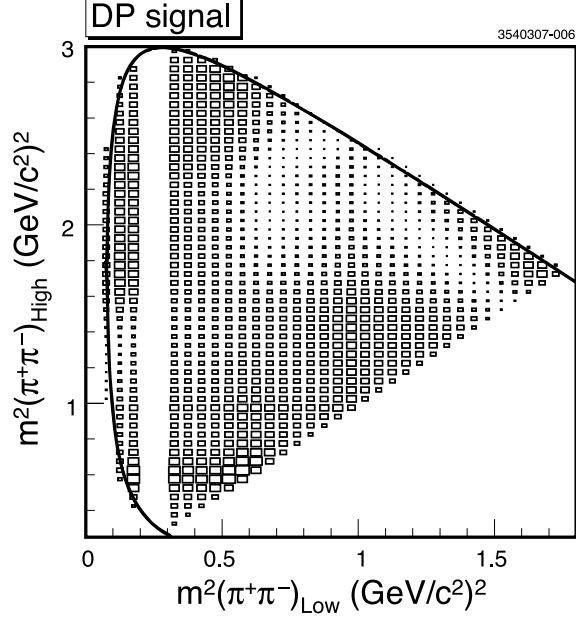


FIG. 7: The signal p.d.f. for the isobar model fit described in the text.

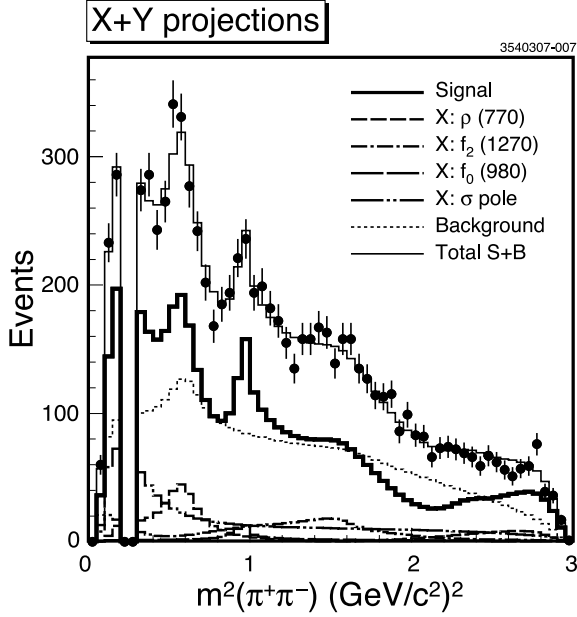


FIG. 8: Projection of the Dalitz plot onto the $m^2(\pi^+\pi^-)$ axis (two combinations per D^+ candidate) for CLEO-c data (points) and isobar model fit (histograms) showing the various components.

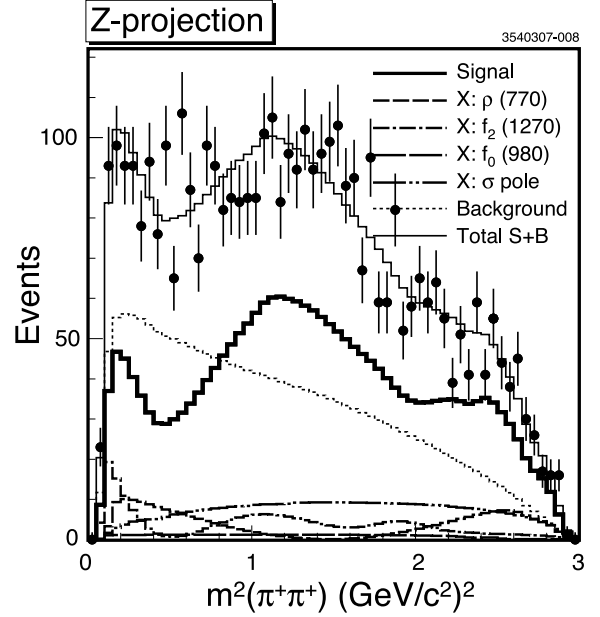


FIG. 9: Projection of the Dalitz plot onto the $m^2(\pi^+\pi^+)$ axis for CLEO-c data (points) and isobar model fit (histograms) showing the various components.

freedom, varying the list of contributions to the Dalitz plot, changing the event selection, and varying the efficiency and background parameterizations. The systematic uncertainty of each fit parameter is estimated as the quadratic sum of the mean and root mean square values of the distribution of the changes in the parameter from its value in the nominal fit. For example for the poorly established resonances $f_0(980)$, $f_0(1370)$, and σ pole, we allow their parameters to float and the variations of the other fit parameters contribute to the systematic errors. The nominal and fitted values of these parameters are presented in Table IV. The fit results when the parameters are allowed to float do not vary from the nominal values by more than two standard deviations.

TABLE IV: Parameters for the poorly established resonances used in the nominal isobar model fit and their fitted values when they are allowed float.

	Parameter	Nominal Value	Fitted Value
Signal fraction	f_{sig} from Eq. 4	0.548	0.552 ± 0.020
$f_0(980)$	$m_{f_0(980)}$ (MeV/ c^2)	965	953 ± 20
	$g_{f_0\pi\pi}$ (MeV/ c^2)	406	329 ± 96
	$g_{f_0K\bar{K}}/g_{f_0\pi\pi}$	2 – fixed	2 – fixed
$f_0(1370)$	$m_{f_0(1370)}$ (MeV/ c^2)	1350	1259 ± 55
	$\Gamma_{f_0(1370)}$ (MeV/ c^2)	265	298 ± 21
σ pole	$Re(m_\sigma)$ (MeV/ c^2)	470	466 ± 18
	$Im(m_\sigma)$ (MeV/ c^2)	-220	-223 ± 28

C. Schechter Model

The isobar model drawbacks are most apparent in the S wave $\pi^+\pi^-$ sector where wide resonances overlap and unitarity is not fulfilled. The model of Joseph Schechter and co-workers in Refs [19], [9] is based on the meson part of the chiral invariant linear sigma model [20] Lagrangian. Poles are handled using K-matrix regularization which respects unitarity by definition. Details of the parameterization are discussed in Appendix VII A, and here we only summarize the meaning of the fit parameters.

In our isobar model Dalitz plot fit the $\pi^+\pi^-$ S wave is represented by a complex pole for the σ , the Flatté for the $f_0(980)$ and two Breit-Wigner for the $f_0(1370)$ and $f_0(1500)$. Schechter’s S wave amplitude, Eq. 22 (Appendix VII A), parameterizes simultaneously the σ mixed with the $f_0(980)$ in strong and weak interactions. The Schechter model describes the mixed σ and $f_0(980)$ contributions to the Dalitz plot with seven parameters: the bare masses m_σ and m_{f_0} ; the strong mixing angle ψ between the σ and $f_0(980)$; the total S wave amplitude a_{SW} and phase ϕ_{SW} ; and the relative weak amplitude a_{f_0} and phase ϕ_{f_0} of the $f_0(980)$ with respect to the σ amplitude. A combination of these parameters in the model gives the total $\pi^+\pi^-$ scattering phase, $\delta(m)$, and an overall S wave amplitude, A_{SW} , for the σ and $f_0(980)$ contributions. Operationally we replace the isobar σ and $f_0(980)$ contributions by the function of Eq. 22 times $c_{SW} = a_{SW}e^{i\phi_{SW}}$. The Breit-Wigner’s parameterization is still used for the $f_0(1370)$ and $f_0(1500)$.

In an initial fit #S1, shown in Table V, we fix all amplitudes and phases to their values from our isobar model fit, fix the S wave model parameters as in Eq. 19, float the S wave

TABLE V: S wave amplitude parameters in the fit of the Schechter model described in the text to the $D^+ \rightarrow \pi^- \pi^+ \pi^+$ Dalitz plot.

Mode	#S1	#S2	#S3
m_σ (MeV/ c^2)	847	758±36	745±55
m_{f_0} (MeV/ c^2)	1300	1385±101	1221±128
ψ (°)	48.6	45±5	38±9
a_{SW}	4.1±0.2	3.9±0.4	4.5±0.6
ϕ_{SW} (°)	54±3	54±4	55±6
a_{f_0}	3.8±0.2	4.2±1.5	2.1±1.5
ϕ_{f_0} (°)	23±3	22±5	21±5
FF (S wave)	45.9±1.9	46.4±4.8	43±12
$\sum_i FF_i$ (%)	92.1	90.6	88.3
Pearson/ $N_{d.o.f.}$	116.3/96	100.4/93	99.6/87
Probability (%)	7.8	28.2	16.8
$-2 \sum \log L$	414	398	397.3

amplitude a_{SW} and phase ϕ_{SW} , and float the relative $f_0(980)$ amplitude a_{f_0} and phase ϕ_{f_0} in Eq. 22. This fit gives a probability of 8% which indicates the Schechter model for the S wave is an acceptable description of the data.

In a second fit, #S2 in Table V, we start from the parameters obtained in #S1 and allow the bare masses m_σ , m_{f_0} , and the strong mixing phase ψ in Eq. 22 to float. This fit gives a probability of 28% and $m_\sigma = (758 \pm 36)$ MeV/ c^2 , which is ~ 3 standard deviations lower than the values obtained in Ref. [19], as also shown in our Eq. 19. The mass m_{f_0} and the phase ψ are statistically consistent with the results in Ref. [19].

Fits #S1 and #S2 are used for an initial assessment of the Schechter S wave parameters relative to the isobar model fit. In a final fit, #S3 in Table V, we float the Schechter S wave model parameters and all the parameters of the other contributions. The results of fit #S3 are shown in Figs. 10 and 11 in projections of the Dalitz plot. Figure 12 shows the isolated S wave contribution to the Dalitz plot, and Fig. 13 shows the $\pi\pi$ scattering phase, $\delta(m)$, defined in Eq. 20 in Appendix VII A. The total signal contribution is very similar to that shown in Fig. 7. Figure 14 shows the complex amplitude A_{SW} from Eq. 22 as the real and imaginary parts, the magnitude and complex phase.

Employing the Schechter model changes the fit parameters for the non S wave contribution by less than the systematic uncertainties in the isobar model fit. We also note that the amplitude and fractions of $f_0(1370)$ and $f_0(1500)$ tend to be larger in the Schechter model fit. This model gives an acceptable fit probability $\sim 17\%$ when it is used to describe the σ and $f_0(980)$ fractions in our data. The S wave fit fraction, $(43 \pm 12)\%$, is consistent with a sum of fit fractions from σ , $(41.8 \pm 1.4 \pm 2.5)\%$, and $f_0(980)$, $(4.1 \pm 0.9 \pm 0.3)\%$ in the isobar model. We find the Schechter S wave model parameters, listed in Table V, are consistent with the values in Ref. [19]. Our data are consistent with both the isobar and Schechter models.

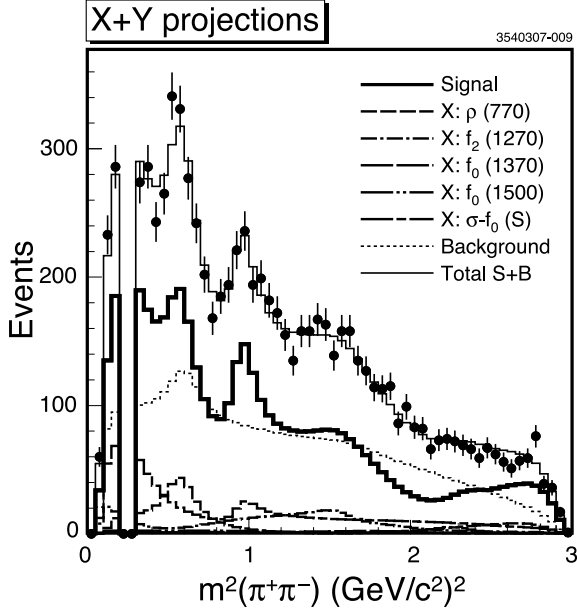


FIG. 10: Projection of the Dalitz plot onto the $m^2(\pi^+\pi^-)$ axis (two combinations per D^+ candidate) for CLEO-c data (points) and Schechter model fit #S3 (histograms) showing the various components.

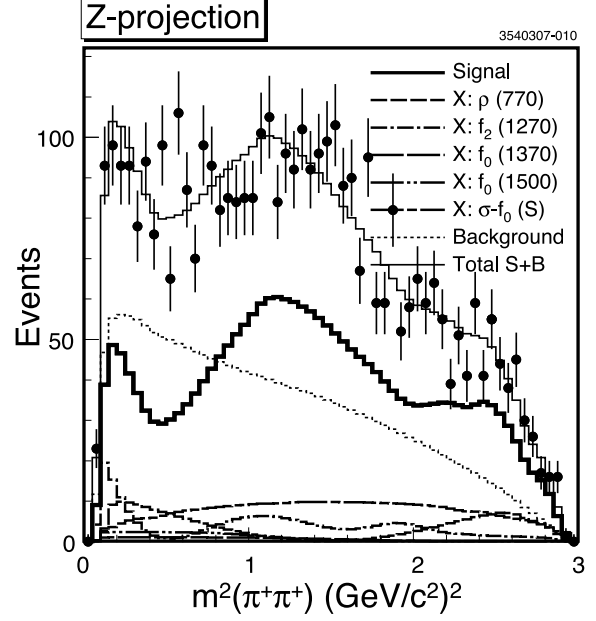


FIG. 11: Projection of the Dalitz plot onto the $m^2(\pi^+\pi^+)$ axis for CLEO-c data (points) and Schechter model fit #S3 (histograms) showing the various components.

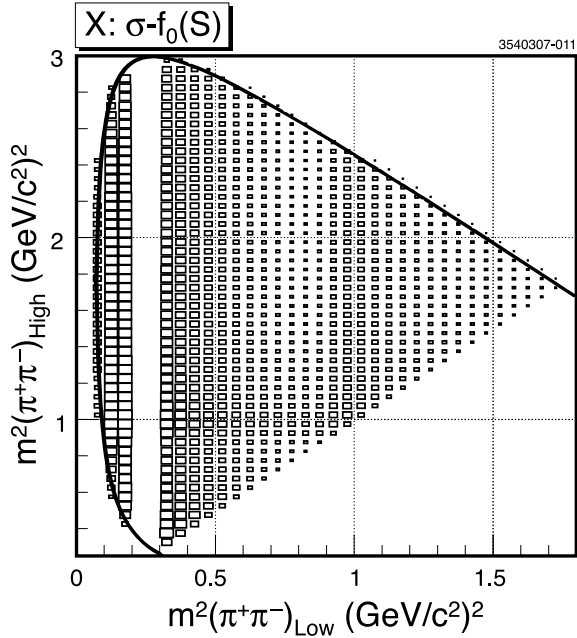


FIG. 12: The isolated S wave contribution of Schechter model fit #S3 on the Dalitz plot.

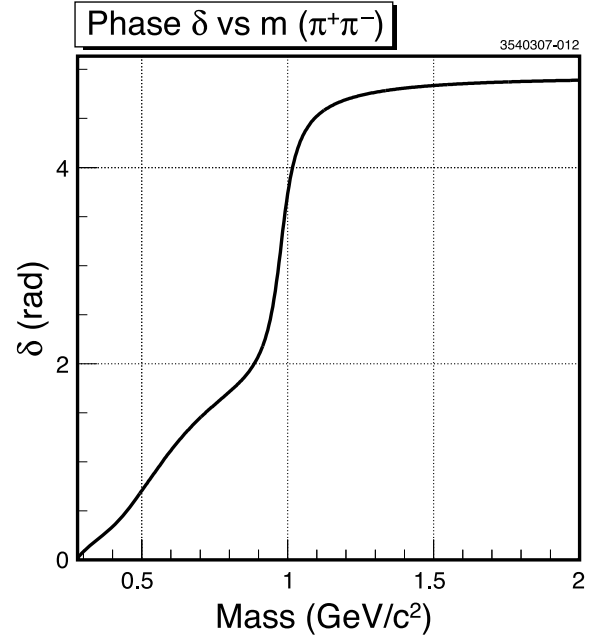


FIG. 13: The $\pi^+\pi^-$ scattering phase $\delta(m)$, Eq. 20, calculated for parameters from Schechter model fit #S3 to the $D^+ \rightarrow \pi^-\pi^+\pi^+$ Dalitz plot.

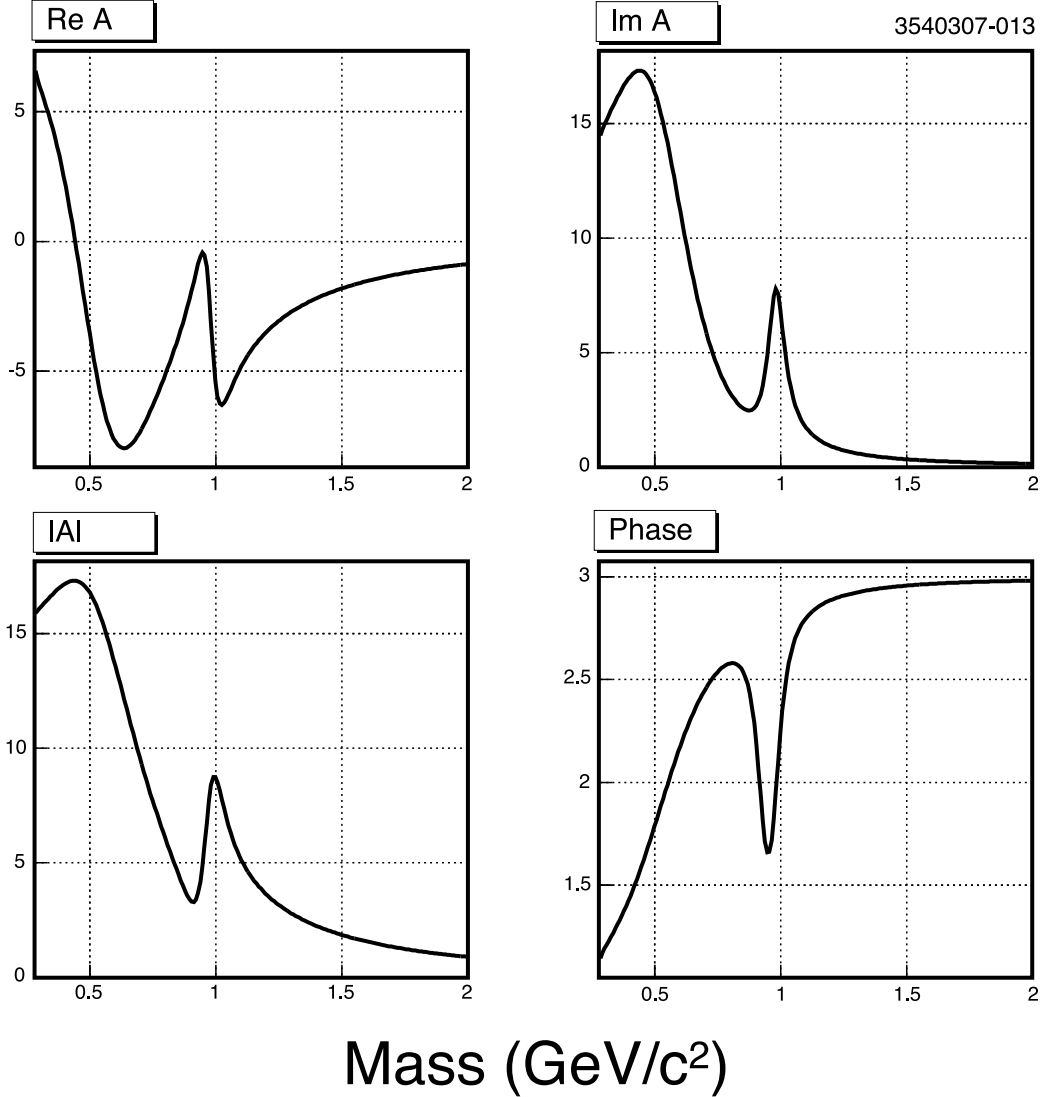


FIG. 14: Complex S wave amplitude from Schechter model fit #S3 to the $D^+ \rightarrow \pi^- \pi^+ \pi^+$ Dalitz plot. The real and imaginary parts, the magnitude and phase are shown as a function of $\pi^+ \pi^-$ mass.

D. Achasov Model

In Refs. [21]–[25] and references therein, a $\pi\pi$ S wave interaction is studied for $\pi\pi \rightarrow \pi\pi$, $\pi\pi \rightarrow K\bar{K}$, $\phi \rightarrow (f_0 - \sigma)\gamma \rightarrow \pi\pi\gamma$, and $\gamma\gamma \rightarrow \pi\pi$ processes in a manner motivated by field theory. The $\pi\pi$ S wave production and the final state interaction (FSI) mechanism in D meson three-body decays have not yet been considered in the framework of this model. In Ref. [10] the $\pi\pi$ S wave amplitude in $D^+ \rightarrow \pi^- \pi^+ \pi^+$ decay is discussed. The developed formalism is described in Appendix VII B, and here we only summarize the meaning of the fit parameters. The Achasov model treats the $\pi\pi$ S wave contribution to $D^+ \rightarrow \pi^- \pi^+ \pi^+$ via the sum of a number of amplitudes. There is a contribution from the non-resonant, point-like $\pi^- \pi^+ \pi^+$ production amplitude; direct resonance production via the $D^+ \rightarrow \sigma \pi^+$, $D^+ \rightarrow f_0(980) \pi^+$; and the rescattering terms from several intermediate states, $\pi^+ \pi^-$, $\pi^0 \pi^0$,

and $K\bar{K}$, to the final $\pi^+\pi^-$ state. Our parameterization has an amplitude, $a_{D^+R\pi^+}$, and phase, $\phi_{D^+R\pi^+}$, for the direct resonance production term, accounting for the σ and f_0 components controlled by the coupling constants $g_{D^+\sigma\pi^+}$ and $g_{D^+f_0\pi^+}$. The contributions from rescattering have amplitudes and phases parametrized by a_{mode} and ϕ_{mode} plus a parameter from loop diagram contributions, d_{mode} . We explicitly fit for the “mode” = $\pi^+\pi^-$, $\pi^0\pi^0$, and $K\bar{K}$ rescattering contributions. The contribution from non-resonant $\pi^-\pi^+\pi^+$ is also accounted for the relevant point-like production amplitude parameter.

We start with the parameters, shown in Table II, where the σ pole and $f_0(980)$ are replaced by the S wave amplitude from Eq. 75. We fix all resonance parameters from our isobar model fit and float different sets of S wave parameters to assess their range. In four fits we float the amplitude, a_{mode} , phase, ϕ_{mode} , and the offset parameter, d_{mode} , (or coupling constants $g_{D^+\sigma\pi^+}$ and $g_{D^+f_0\pi^+}$ in case of direct σ or f_0 meson production) for sub-modes $\pi^+\pi^- \rightarrow \pi^+\pi^-$, $K\bar{K} \rightarrow \pi^+\pi^-$, $\pi^0\pi^0 \rightarrow \pi^+\pi^-$, or “ $DR\pi$ ”, respectively. For each of the single sub-modes we get a fit inconsistent with data. In five fits we float a_{mode} , ϕ_{mode} , d_{mode} (or $g_{D^+\sigma\pi^+}$ and $g_{D^+f_0\pi^+}$) parameters for each combination of two sub-modes. All fits without the $\pi^0\pi^0 \rightarrow \pi^+\pi^-$ sub-mode show probability of consistency with the data $\sim 10\%$, while models with the $\pi^0\pi^0 \rightarrow \pi^+\pi^-$ sub-mode are poorly consistent with the data. In three fits we include three or more sub-modes. These have a consistency with the data of $\sim 10\%$, but give poor statistical significance for the amplitude parameters. Fit #A1 allows full freedom for all the S wave sub-modes and gives a probability of consistency with the data of $\sim 19\%$, with 2–3 standard deviation significance for the amplitude parameters. Its results are shown in Table VI.

We begin again with parameters of Fit #A1 and float or set to zero amplitude the parameters of the $f_2(1270)$, $f_0(1370)$, and $f_0(1500)$ contributions from our isobar fit. In Fit #A2 we float all the S wave parameters and all resonance parameters for the $f_2(1270)$, $f_0(1370)$, and $f_0(1500)$ contributions. Variations of the nominal fit parameters, shown in Table II, are within the range of the isobar model uncertainties. Fit #A3 is like Fit #A2, but the contributions from $f_0(1370)$ and $f_0(1500)$ scalar resonances are set to zero. The fit quality change from Fit #A2 to Fit #A3 is small. The S wave of the Achasov model has enough freedom to substitute for the contribution of the $f_0(1370)$ and $f_0(1500)$ resonances. The results of these two fits are shown in Table VI. The results of Fit #A2 are shown in Figs. 15–17 giving the Dalitz plot projections onto the $m^2(\pi^+\pi^-)$ and $m^2(\pi^+\pi^+)$ axes, and the representation of the S wave complex amplitude. Our data are consistent with the isobar, Schechter, and Achasov models.

E. Discussion of Models

We have tested three models of the low mass $\pi^+\pi^-$ S wave in $D^+ \rightarrow \pi^-\pi^+\pi^+$, and we find little variation of the parameters describing non S wave contributions. The fit gives similar S wave contributions for all three models. We show this by plotting the relevant complex functions describing the S wave. Figure 18 shows the Flatté and the complex-pole parameterizations for $f_0(980)$ and σ , respectively, for our isobar model fit to the data. Figure 14 shows the results of the Schechter model fit, and Fig. 17 shows the results of the Achasov model fit. In Figs. 19, 20 we compare the $\pi\pi$ S wave amplitude and phase in the accessible mass region from threshold to $1.7 \text{ GeV}/c^2$ for these three models. The solid curve corresponds to the Schechter model fit to our Dalitz plot, the dashed curve is for Achasov model fit, and the $\pm 1\sigma$ of the amplitude and phase parameters range of the S wave

TABLE VI: Fit results for the Achasov model as described in the text.

Sub-amplitude, parameters	#A1	#A2	#A3
$DR\pi$			
$a_{D^+R\pi^+}$	1-fixed	1-fixed	1-fixed
$\phi_{D^+R\pi^+}$ ($^\circ$)	-3 ± 32	-66 ± 7	-92 ± 13
$g_{D^+\sigma\pi^+}$	24 ± 11	39 ± 8	21 ± 12
$g_{D^+f_0\pi^+}$	27 ± 11	267 ± 24	132 ± 44
$\pi^+\pi^\pm \rightarrow \pi^+\pi^\pm$			
$a_{\pi\pi}$	0.25 ± 0.08	0.31 ± 0.04	0.25 ± 0.07
$\phi_{\pi\pi}$ ($^\circ$)	104 ± 12	70 ± 9	93 ± 9
$d_{\pi\pi}$	1.5 ± 0.3	2.2 ± 0.2	2.9 ± 0.3
$K\bar{K} \rightarrow \pi^+\pi^-$			
$a_{K\bar{K}}$	0.56 ± 0.39	1.35 ± 0.15	1.80 ± 0.40
$\phi_{K\bar{K}}$ ($^\circ$)	110 ± 24	107 ± 7	81 ± 12
$d_{K\bar{K}}$	0.02 ± 0.21	0.90 ± 0.09	0.37 ± 0.10
$\pi^0\pi^0 \rightarrow \pi^+\pi^-$			
$a_{\pi^0\pi^0}$	0.13 ± 0.07	0.11 ± 0.03	0.06 ± 0.05
$\phi_{\pi^0\pi^0}$ ($^\circ$)	41 ± 31	149 ± 23	0 ± 41
$d_{\pi^0\pi^0}$	$= d_{\pi\pi}$	$= d_{\pi\pi}$	$= d_{\pi\pi}$
Fit fractions (%)			
$\sum_i FF_i$	112.3	140.4	117.1
$\pi^+\pi^-, 2\times$	32.1 ± 9.8	37.5 ± 3.6	34.2 ± 5.3
$\pi^+\pi^+$	6.1 ± 5.0	16.6 ± 3.2	9.9 ± 3.0
Fit goodness			
$Pearson/n_{d.o.f.}$	100.7/89	96.9/83	106.8/87
Probability (%)	18.7	14.1	7.3
$-2\sum \log L$	398.6	394.7	405.1

contribution in the isobar model is indicated by the two dotted curves. The S wave shapes are quite similar up to the interplay with other resonances, and with the data set we have in hand we are not sensitive to the details of the S wave parameterization.

V. SUMMARY

Using a sample of 0.78 million $e^+e^- \rightarrow \psi(3770) \rightarrow D^+D^-$ events collected in the CLEO-c experiment, we performed a Dalitz plot analysis of the $D^+ \rightarrow \pi^-\pi^+\pi^+$ decay. Our nominal results, obtained within the framework of the isobar model and shown in Table II, reinforce the previous conclusion [3], [4] that a sizable $\sigma\pi^+$ component is required, in addition to other intermediate states $\rho(770)\pi^+$, $f_2(1270)\pi^+$, $f_0(1370)\pi^+$, $f_0(1500)\pi^+$, and $f_0(980)\pi^+$, in order to describe the $D^+ \rightarrow \pi^-\pi^+\pi^+$ decay. The systematic uncertainties are estimated by varying the fit parameters from their nominal values. We also show in Table IV a set of optimal

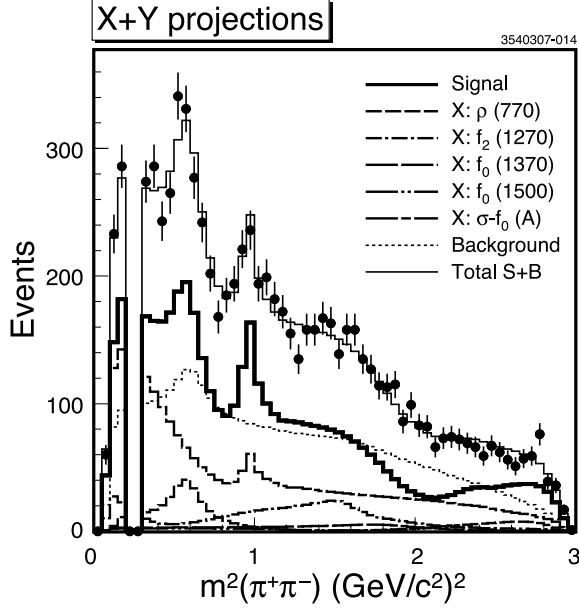


FIG. 15: Projection of the Dalitz plot onto the $m^2(\pi^+\pi^-)$ axis (two combinations per D^+ candidate) for CLEO-c data (points) and Achasov model fit #A2 (histograms) showing the various components.

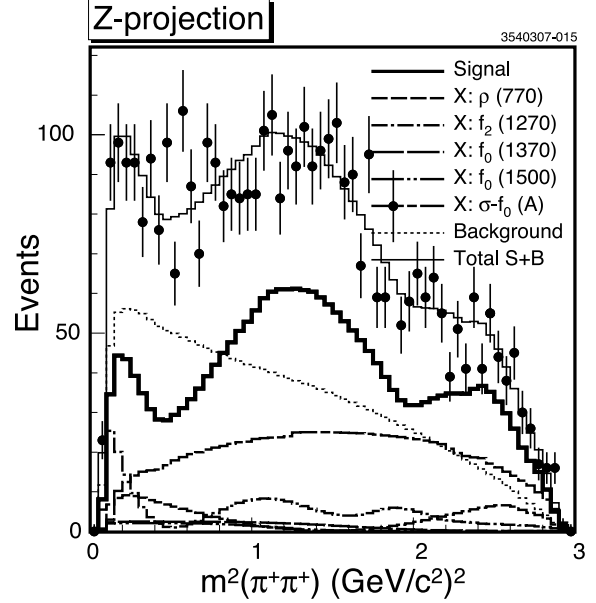


FIG. 16: Projection of the Dalitz plot onto the $m^2(\pi^+\pi^+)$ axis for CLEO-c data (points) and Achasov model fit #A2 (histograms) showing the various components.

parameters for the σ , $f_0(980)$, and $f_0(1370)$ resonances based on our isobar model fit to the $D^+ \rightarrow \pi^-\pi^+\pi^+$ Dalitz plot. Limits on contributions from $\rho(1450)\pi^+$, non-resonant, I=2 $\pi^+\pi^+$ S wave, $f_0(1710)\pi^+$, and $f_0(1790)\pi^+$, shown in Table III, are set at 95% confidence level.

We tested other models of the low mass $\pi\pi$ S wave contributions and in each case obtain optimal parameters. In Table V we summarize results for the model suggested by J. Schechter and co-workers [9], [19]. All fits for this model show consistent values for the parameters. We also apply the S wave model suggested by N.N. Achasov *et al.* [10]. This model has more freedom in sub-modes than we are confidently able to define with our data. Possible solutions are presented in Table VI. Further progress with this model can be achieved if several D meson decay modes with higher statistics are analyzed simultaneously.

For all $\pi\pi$ S wave models we find that their fit fraction exceeds 50%, and confirm results of previous experiments of a significant contribution from a low mass $\pi^+\pi^-$ S wave in the $D^+ \rightarrow \pi^-\pi^+\pi^+$ decay. Table VII compares the fit fractions from the fits to the three models described above. The S wave fit fraction in Achasov model is three standard deviation larger than in the Isobar and Schechter model. The sum of all fit fractions is also larger in Achasov model, that indicates on difference in interference terms. The fit fractions for sub-modes are consistent between these three models. Figures 19 and 20 compare the amplitude and phase, respectively, for the $\pi^+\pi^-$ S wave contribution we have found in the three considered models. With our given data sample all three S wave parameterizations adequately describe the $D^+ \rightarrow \pi^-\pi^+\pi^+$ Dalitz plot.

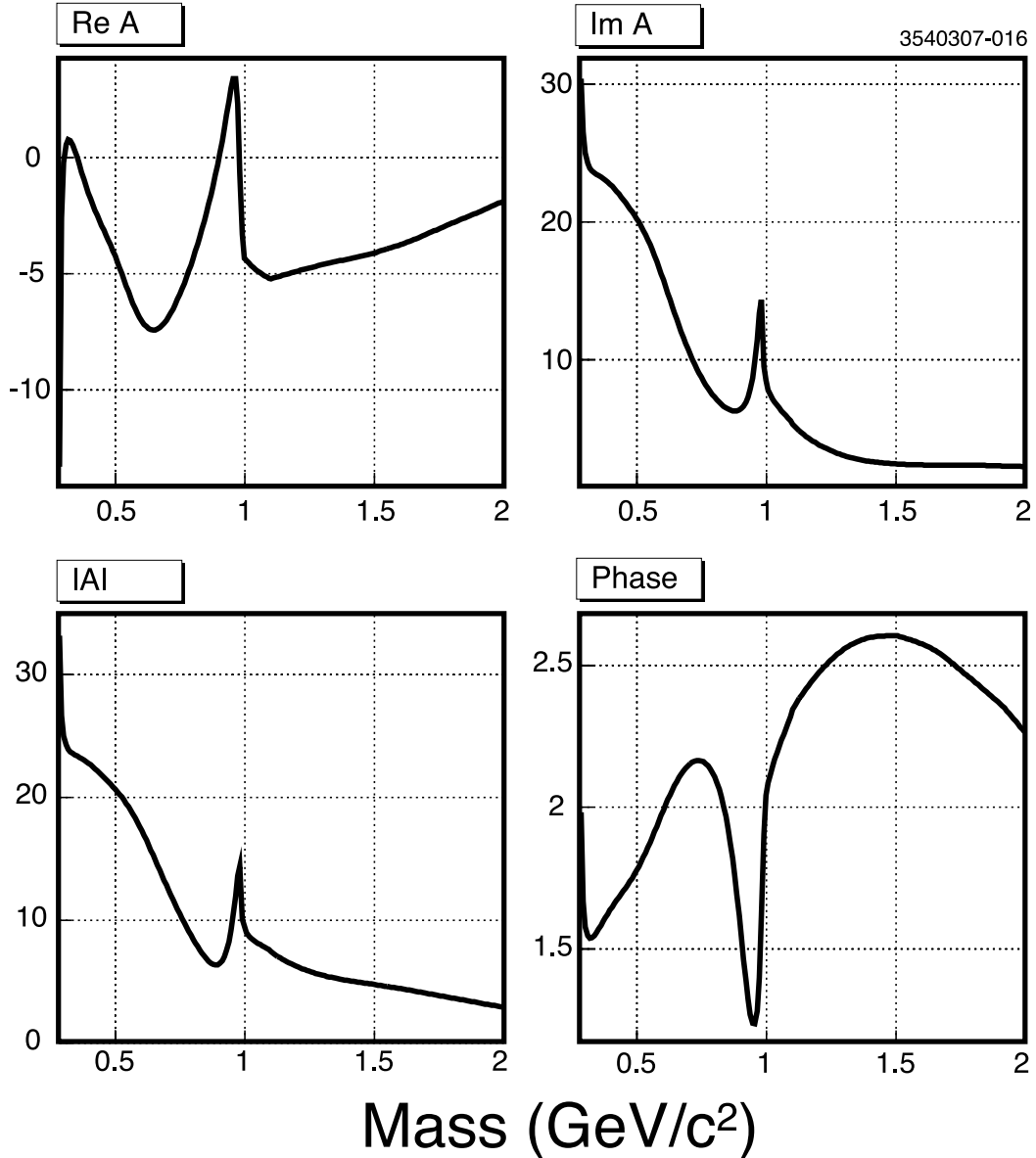


FIG. 17: Complex S wave amplitude from Achasov model fit #A2 to the $D^+ \rightarrow \pi^- \pi^+ \pi^+$ Dalitz plot. The real and imaginary parts, the magnitude and phase are shown as a function of $\pi^+ \pi^-$ mass.

VI. ACKNOWLEDGMENTS

We thank Joseph Schechter, Amir Fariborz, and Nikolay Achasov for stimulating discussions and significant help in application of the low mass $\pi\pi$ S wave models. We gratefully acknowledge the effort of the CESR staff in providing us with excellent luminosity and running conditions. D. Cronin-Hennessy and A. Ryd thank the A.P. Sloan Foundation. This work was supported by the National Science Foundation, the U.S. Department of Energy, and the Natural Sciences and Engineering Research Council of Canada.

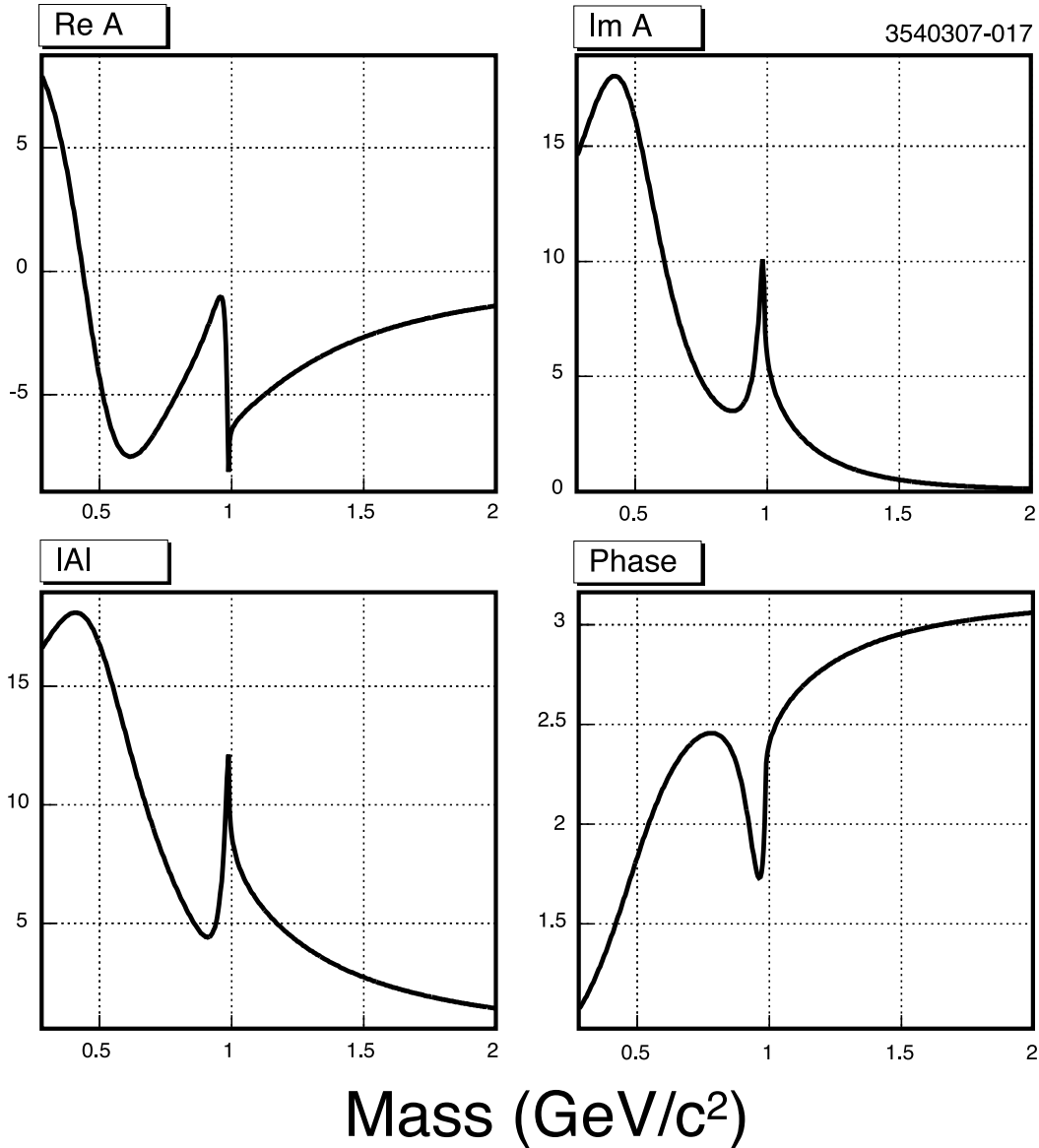


FIG. 18: Complex S wave amplitude (complex pole for σ and Flatté for $f_0(980)$) from isobar model fit to the $D^+ \rightarrow \pi^- \pi^+ \pi^+$ Dalitz plot. The real and imaginary parts, the magnitude and phase are shown as a function of $\pi^+ \pi^-$ mass.

VII. APPENDIX: ALTERNATIVE MODELS OF THE $\pi\pi$ S WAVE

A. Formalism of the $\pi\pi$ S wave suggested by J. Schechter

A tree level $\pi\pi \rightarrow \pi\pi$ scattering amplitude for two resonances σ and $\tilde{\sigma}$ strongly-mixed with phase ψ is given in Eq. 3.2 of Ref. [19]:

$$T_{0\ tree}^0 = \cos^2 \psi \left[\alpha(s) + \frac{\beta(s)}{m_\sigma^2 - s} \right] + \sin^2 \psi \left[\tilde{\alpha}(s) + \frac{\tilde{\beta}(s)}{m_{\tilde{\sigma}}^2 - s} \right], \quad (9)$$

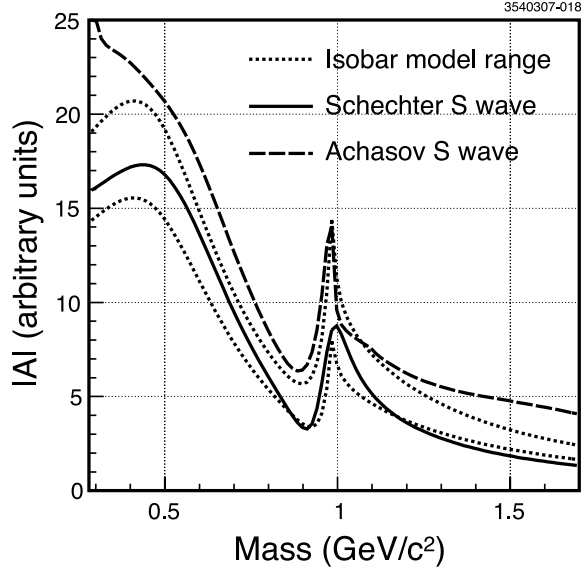


FIG. 19: The $\pi^+\pi^-$ S wave absolute amplitude for different models.

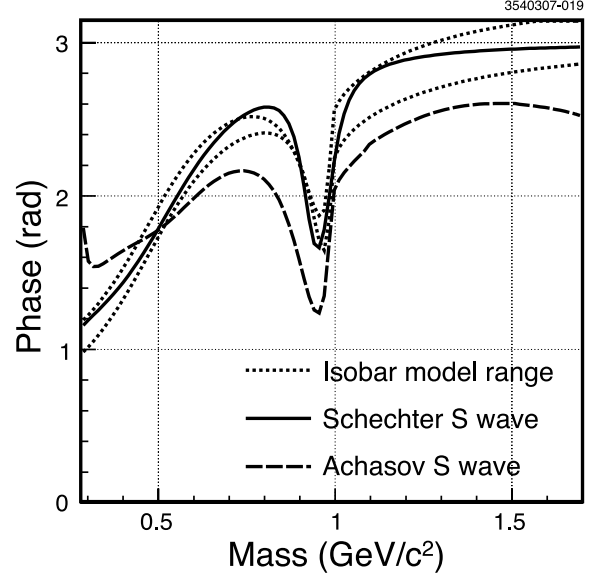


FIG. 20: The $\pi^+\pi^-$ S wave phase for different models.

TABLE VII: A comparison of the observed fit fractions (FF) in % in the three models of $D^+ \rightarrow \pi^-\pi^+\pi^+$. For the “Isobar” column, the “Low S wave π^+ ” entry is the sum of the two entries above.

Mode	Isobar	Schechter #S3	Achasov #A2
$\sigma\pi^+$	41.8 ± 2.9		
$f_0(980)\pi^+$	4.1 ± 0.9		
Low S wave π^+	45.9 ± 3.0	43.4 ± 11.8	75 ± 7
$f_0(1370)\pi^+$	2.6 ± 1.9	2.6 ± 1.7	3.2 ± 0.7
$f_0(1500)\pi^+$	3.4 ± 1.3	4.3 ± 2.4	4.0 ± 0.8
$\rho^0(770)\pi^+$	20.0 ± 2.5	19.6 ± 7.4	18.4 ± 4.0
$f_2(1270)\pi^+$	18.2 ± 2.7	18.4 ± 7.4	23.2 ± 5.0
I=2 $\pi^+\pi^+$ S wave			16.6 ± 3.2
$\sum_i FF_i$	90.1	88.3	140.4

where

$$\alpha(s) = \frac{\sqrt{1 - \frac{4m_\pi^2}{s}}}{16\pi F_\pi^2} (m_\sigma^2 - m_\pi^2) \left[-5 + 2 \frac{m_\sigma^2 - m_\pi^2}{s - 4m_\pi^2} \ln \left(\frac{m_\sigma^2 + s - 4m_\pi^2}{m_\sigma^2} \right) \right], \quad (10)$$

$$\beta(s) = \frac{3\sqrt{1 - \frac{4m_\pi^2}{s}}}{16\pi F_\pi^2} (m_\sigma^2 - m_\pi^2)^2, \quad (11)$$

s is the $\pi^+\pi^-$ invariant mass squared, m_π and $F_\pi=0.131$ GeV are the pion mass and the decay constant, m_σ and $m_{\tilde{\sigma}}$ are the bare masses of two scalar resonances, and ψ is a strong mixing angle. We use the original notation of Ref. [19], the tilde is used for all parameters relating to the second scalar resonance, $\tilde{\sigma}$, which in our case is associated with $f_0(980)$. Equation 9 can be re-written as

$$T_{0\ tree}^0 = A + \frac{B}{P}, \quad (12)$$

where

$$A = \alpha \cos^2 \psi + \tilde{\alpha} \sin^2 \psi, \quad (13)$$

$$B = \beta \cdot (m_\sigma^2 - s) \cos^2 \psi + \tilde{\beta} \cdot (m_\sigma^2 - s) \sin^2 \psi, \quad (14)$$

$$P = (m_\sigma^2 - s)(m_{f_0}^2 - s). \quad (15)$$

According to the Dyson equation for the $\pi\pi$ scattering, Eq. 3.3 from Ref. [19] gives an expression for a total scattering amplitude through the tree amplitude:

$$T_0^0(s) = \frac{T_{0 \text{ tree}}^0(s)}{1 - iT_{0 \text{ tree}}^0(s)}. \quad (16)$$

The scattering amplitude is a complex number, $T_0^0(s) = |T_0^0(s)|e^{i\delta(s)}$, then the tree amplitude can be associated with the tangent of the scattering phase,

$$T_{0 \text{ tree}}^0(s) = \tan \delta(s), \quad (17)$$

and we get an expression for $\cos \delta$:

$$\cos \delta = \frac{1}{\sqrt{1 + \tan^2 \delta}} = \frac{P}{\sqrt{P^2 + (P \cdot A + B)^2}}. \quad (18)$$

Expression $\delta(s) = \arctan(T_{0 \text{ tree}}^0(s))$ defines a scattering phase in the range $[-\frac{\pi}{2}, \frac{\pi}{2}]$. This phase $\delta(s)$ has two discontinuities at $s = m_\sigma^2$ and $s = m_{f_0}^2$ for parameters taken from Ref. [19],

$$m_\sigma = 0.847 \text{ GeV}/c^2, \quad m_{f_0} = 1.30 \text{ GeV}/c^2, \quad \psi = 48.6^\circ. \quad (19)$$

In order to remove discontinuities we add a phase-shift $+\pi$ above each bare mass:

$$\delta(s) = \arctan(T_{0 \text{ tree}}^0(s)) + \pi(\theta(s - m_\sigma^2) + \theta(s - m_{f_0}^2)), \quad (20)$$

where $\theta(x)$ is a step function, that makes the phase smooth, as shown in Fig. 13.

In this model the production amplitude is obtained from the total scattering amplitude, Eq. 16, by replacing the first tree level $\pi\pi \rightarrow \pi\pi$ scattering diagram amplitude, $T_{0 \text{ tree}}^0$, by the resonance propagator $(m_\sigma^2 - s)^{-1}$ with the coupling constant $g_{\sigma\pi\pi}$ and keeping the proper re-scattering amplitude, represented by the ‘‘bubble sum’’ factor $(1 - iT_{0 \text{ tree}}^0)^{-1}$:

$$\mathcal{A}_\sigma = \frac{g_{\sigma\pi\pi}}{m_\sigma^2 - s} \cdot \frac{1}{1 - iT_{0 \text{ tree}}^0} = \frac{g_{\sigma\pi\pi}}{m_\sigma^2 - s} \cdot \cos \delta \cdot e^{i\delta}. \quad (21)$$

Extending Eq. 21 (Eq. 15 from Ref. [9]) for the case of two resonances σ and $f_0(980)$ we get the total production amplitude with relative weak interaction mixing factor $a_{f_0}e^{i\phi_{f_0}}$

$$A_{SW} = \mathcal{A}_\sigma + \mathcal{A}_{f_0} = \cos \delta \cdot e^{i\delta} \left[\frac{1}{m_\sigma^2 - s} + \frac{a_{f_0}e^{i\phi_{f_0}}}{m_{f_0}^2 - s} \right]. \quad (22)$$

Note, that Eq. 22 does not contain singular terms because both poles are contracted into the P factor from $\cos \delta$, Eq. 15 and 18. For the first iteration we set

$$a_{f_0} = 1, \quad \phi_{f_0} = 0^\circ. \quad (23)$$

It should be noted, that in the frame of this model, σ is a scalar $\pi\pi$ resonance which has a bare mass m_σ as a parameter. The bare mass does not coincide with a peak position as in case of Breit-Wigner, that is clearly seen in Eq. 19 for the mass of $f_0(980)$. This simple model does not take in to account that the scalar resonances may have other decay modes, coupled channels. For example, it is well known that $f_0(980)$ has a $K\bar{K}$ decay mode with a mass dependent rate as large as $\sim 20\%$. Presumably, this amplitude, obtained from the chiral Lagrangian, works well in the region close to the production threshold. In the case of SU(3) symmetry it accounts for the two low mass resonances σ and $f_0(980)$. Other higher mass resonances such as the $f_0(1370)$ and $f_0(1500)$ are not taken into account. These issues restrict the precision and limit the application of this model.

B. Formalism of the $\pi\pi$ S wave suggested by N.N. Achasov

1. $D^+ \rightarrow \pi^- \pi^+ \pi^+$ total amplitude

In this section we summarize a suggested formalism [10] for a parameterization of the $\pi\pi$ scalar amplitude in the $D^+ \rightarrow \pi^- \pi^+ \pi^+$ decay, and present the details of our implementation in the Dalitz plot fitter with some relevant cross-checks. For the $D^+ \rightarrow \pi^- \pi^+ \pi^+$ decay Ref.[10] suggests the use of a $\pi\pi$ S wave amplitude that is a superposition

$$\begin{aligned}
A(D^+ \rightarrow \pi_1^+ \pi_2^+ \pi^-) &= A^{pl}(D^+ \rightarrow \pi_1^+ \pi_2^+ \pi^-) \\
&+ B[D^+ \rightarrow \pi_1^+(\pi_2^+ \pi^- \rightarrow \pi_2^+ \pi^-) \rightarrow \pi_1^+ \pi_2^+ \pi^-] + B[1 \leftrightarrow 2] \\
&+ E[D^+ \rightarrow (\pi_1^+ \pi_2^+ \rightarrow \pi_1^+ \pi_2^+) \pi^- \rightarrow \pi_1^+ \pi_2^+ \pi^-] \\
&+ F[D^+ \rightarrow \pi_1^+(\sigma + f_0) \rightarrow \pi_1^+ \pi_2^+ \pi^-] + F[1 \leftrightarrow 2] \\
&+ \bar{B}[D^+ \rightarrow \pi_1^+(\pi^0 \pi^0 \rightarrow \pi_2^+ \pi^-) \rightarrow \pi_1^+ \pi_2^+ \pi^-] + \bar{B}[1 \leftrightarrow 2] \\
&+ C[D^+ \rightarrow \pi_1^+(K^+ K^- \rightarrow \pi_2^+ \pi^-) \rightarrow \pi_1^+ \pi_2^+ \pi^-] + C[1 \leftrightarrow 2] \\
&+ \bar{C}[D^+ \rightarrow \pi_1^+(K^0 \bar{K}^0 \rightarrow \pi_2^+ \pi^-) \rightarrow \pi_1^+ \pi_2^+ \pi^-] + \bar{C}[1 \leftrightarrow 2].
\end{aligned} \tag{24}$$

of a point-like, A^{pl} , direct resonance, F , and non-resonant production terms, B , C , E , followed by the re-scattering in to the $\pi\pi$ final state. Here we list the definitions of all the sub-amplitudes in Eq. 24.

The point-like $D^+ \rightarrow \pi_1^+ \pi_2^+ \pi^-$ amplitude is associated with a constant a :

$$A^{pl}(D^+ \rightarrow \pi_1^+ \pi_2^+ \pi^-) = 16\pi a. \tag{25}$$

After the point-like production one would expect $\pi_1^+ \pi^- \rightarrow \pi_1^+ \pi^-$ and $\pi_2^+ \pi^- \rightarrow \pi_2^+ \pi^-$ scattering, which we parametrize as a mass dependent amplitude

$$\begin{aligned}
B[D^+ \rightarrow \pi_1^+(\pi_2^+ \pi^- \rightarrow \pi_2^+ \pi^-) \rightarrow \pi_1^+ \pi_2^+ \pi^-, m = m_{\pi_2^+ \pi^-}] \\
= L_{\pi^+ \pi^-}(m|a, p) \cdot \left(\frac{2}{3} T_0^0(m) + \frac{1}{3} T_0^2(m) \right).
\end{aligned} \tag{26}$$

Functions $L_{\pi^+ \pi^-}(m|a, p)$, $T_0^0(m)$, and $T_0^2(m)$ are described below. An exotic I=2 S wave $\pi_1^+ \pi_2^+ \rightarrow \pi_1^+ \pi_2^+$ scattering is discussed in Ref. [17]

$$E[D^+ \rightarrow (\pi_1^+ \pi_2^+ \rightarrow \pi_1^+ \pi_2^+) \pi^-, m = m_{\pi^+ \pi^+}] = L_{\pi^+ \pi^+}(m|a, r) \cdot T_0^2(m). \tag{27}$$

It is assumed that the σ and f_0 mesons can be produced directly in the $D^+ \rightarrow \pi^+\sigma$ and $D^+ \rightarrow \pi^+f_0$ decays (we use the “ $DR\pi$ ” notation), with an amplitude of

$$F[D^+ \rightarrow \pi_1^+(\sigma + f_0) \rightarrow \pi_1^+\pi_2^+\pi^-, m = m_{\pi_2^+\pi^-}] = T_0^0{}^{res}_{D^+R\pi^+}(m). \quad (28)$$

The point-like $D^+ \rightarrow \pi^+\pi^0\pi^0$ amplitude is associated with another constant \bar{a}

$$A^{pl}(D^+ \rightarrow \pi^+\pi^0\pi^0) = 16\pi\bar{a}. \quad (29)$$

Subsequent $\pi^0\pi^0 \rightarrow \pi^+\pi^-$ rescattering may also contribute to the final state via the amplitude

$$\begin{aligned} \bar{B}[D^+ \rightarrow \pi_1^+(\pi^0\pi^0 \rightarrow \pi_2^+\pi^-) \rightarrow \pi_1^+\pi_2^+\pi^-, m = m_{\pi^0\pi^0}] \\ = L_{\pi^0\pi^0}(m|\bar{a}, q) \cdot \left(\frac{2}{3}T_0^0(m) - \frac{2}{3}T_0^2(m) \right). \end{aligned} \quad (30)$$

In the above equations we assume that $q = r = p$.

The point-like production amplitudes for $D^+ \rightarrow \pi^+K^+K^-$ and $D^+ \rightarrow \pi^+K^0\bar{K}^0$ are represented by the constants c and \bar{c} ,

$$A^{pl}(D^+ \rightarrow \pi^+K^+K^-) = 16\pi c. \quad (31)$$

$$A^{pl}(D^+ \rightarrow \pi^+K^0\bar{K}^0) = 16\pi\bar{c}. \quad (32)$$

Then, two terms account for the relevant rescattering amplitudes $K^+K^- \rightarrow \pi^+\pi^-$ and $K^0\bar{K}^0 \rightarrow \pi^+\pi^-$,

$$\begin{aligned} C[D^+ \rightarrow \pi_1^+(K^+K^- \rightarrow \pi_2^+\pi^-) \rightarrow \pi_1^+\pi_2^+\pi^-, m = m_{K^+K^-}] \\ = L_{K^+K^-}(m|c, s) \cdot T_0^0(K^+K^- \rightarrow \pi^+\pi^-, m), \end{aligned} \quad (33)$$

$$\begin{aligned} \bar{C}[D^+ \rightarrow \pi_1^+(K^0\bar{K}^0 \rightarrow \pi_2^+\pi^-) \rightarrow \pi_1^+\pi_2^+\pi^-, m = m_{K^0\bar{K}^0}] \\ = L_{K^0\bar{K}^0}(m|\bar{c}, t) \cdot T_0^0(K^0\bar{K}^0 \rightarrow \pi^+\pi^-, m), \end{aligned} \quad (34)$$

where we assume that offset parameters are equal, $t = s$.

In above equations we use the function $L_{a\bar{a}}(m|c, d)$, which represents a contribution from the loop diagram

$$L_{a\bar{a}}(m|c, d) = 16\pi c \cdot \begin{cases} i\rho_{a\bar{a}}(m) + \rho_{a\bar{a}}(m)\frac{1}{\pi} \ln \frac{1-\rho_{a\bar{a}}(m)}{1+\rho_{a\bar{a}}(m)} + d, & m \geq 2m_a, \\ -|\rho_{a\bar{a}}(m)| + |\rho_{a\bar{a}}(m)|\frac{2}{\pi} \arctan |\rho_{a\bar{a}}(m)| + d, & m < 2m_a, \end{cases} \quad (35)$$

where

$$|\rho_{a\bar{a}}(m)| = \sqrt{4m_a^2/m^2 - 1}, \quad (36)$$

$$\rho_{a\bar{a}}(m) = \sqrt{1 - 4m_a^2/m^2}. \quad (37)$$

Below all definitions, required for parametrization of the amplitude in our case, are rewritten from the recent Ref. [25].

2. $T_0^0 \equiv T_0^0(\pi\pi \rightarrow \pi\pi, m)$

Equation 23 from Ref. [25] gives the S wave amplitude T_0^0 of $\pi\pi \rightarrow \pi\pi$ scattering with $I=0$ is

$$T_0^0 \equiv T_0^0(\pi\pi \rightarrow \pi\pi, m) = \frac{\eta_0^0 e^{2i\delta_0^0} - 1}{2i\rho_{\pi\pi}(m)} = \frac{e^{2i\delta_B^{\pi\pi}} - 1}{2i\rho_{\pi\pi}(m)} + e^{2i\delta_B^{\pi\pi}} \cdot T_0^0{}^{res}(m). \quad (38)$$

Equation 24 from Ref. [25] gives the total phase

$$\delta_0^0 = \delta_0^0(m) = \delta_B^{\pi\pi}(m) + \delta_{res}(m). \quad (39)$$

Equation 25 from Ref. [25] defines the resonant part of the S matrix

$$S_0^0{}^{res}(m) = \eta_0^0(m) e^{2i\delta_{res}(m)} = 1 + 2i\rho_{\pi\pi}(m) \cdot T_0^0{}^{res}(m), \quad (40)$$

which can be described by the inelasticity

$$\eta_0^0(m) = |S_0^0{}^{res}(m)| \quad (41)$$

and resonant phase

$$\delta_{res}(m) = \frac{1}{2} \cdot \arctan\left(\frac{\Im(S_0^0{}^{res})}{\Re(S_0^0{}^{res})}\right). \quad (42)$$

The chiral background shielding phase $\delta_B^{\pi\pi}(m)$, motivated by the σ model, is taken as Eq. 26 from Ref. [25]:

$$\tan \delta_B^{\pi\pi} = -\frac{p_\pi}{m_\pi} \left(b_0 - b_1 \frac{p_\pi^2}{m_\pi^2} + b_2 \frac{p_\pi^4}{m_\pi^4} \right) \times \frac{1}{1 + (2p_\pi)^2/\Lambda^2}, \quad (43)$$

where $2p_\pi = \sqrt{m^2 - 4m_\pi^2}$, and $(1 + (2p_\pi)^2/\Lambda^2)^{-1}$ is a cutoff factor. The value of parameters b_0 , b_1 , b_2 , and Λ used in our fits are listed in Table VIII. The background phase is derived from Eq. 43

$$\delta_B^{\pi\pi} = \arctan[\tan \delta_B^{\pi\pi}]. \quad (44)$$

3. Resonance amplitudes $T_0^0{}_{D^+R\pi^+}{}^{res}(m)$ and $T_0^0{}^{res}(m)$

In Eq. 28, 38, and 40 we use a brief notation for the production and scattering resonance amplitudes expressed through the mixing matrix operator $G_{RR'}^{-1}$

$$T_0^0{}_{D^+R\pi^+}{}^{res} = e^{i\delta_B^{\pi\pi}(m)} \sum_{RR'} \frac{g_{D^+R\pi^+} G_{RR'}^{-1} g_{R'\pi^+\pi^-}}{16\pi}, \quad (45)$$

$$T_0^0{}^{res} = \sum_{RR'} \frac{g_{R\pi\pi} G_{RR'}^{-1} g_{R'\pi\pi}}{16\pi}. \quad (46)$$

Note the difference between specific coupling constants and the exponential factor in Eqs. 45 and 46.

4. $T_0^0(K\bar{K} \rightarrow \pi\pi, m)$

The S wave amplitude of $K\bar{K} \rightarrow \pi\pi$ scattering, taking in to account mixing through RR' resonances (i.e. σ and $f_0(980)$ mesons) is given by Eq. 3 from Ref. [25]:

$$T_0^0(K^+K^- \rightarrow \pi^+\pi^-, m) = e^{i\delta_B} \sum_{RR'} \frac{g_{RK^+K^-} G_{RR'}^{-1} g_{R'\pi^+\pi^-}}{16\pi}, \quad (47)$$

$$T_0^0(K^0\bar{K}^0 \rightarrow \pi^+\pi^-, m) = e^{i\delta_B} \sum_{RR'} \frac{g_{RK^0\bar{K}^0} G_{RR'}^{-1} g_{R'\pi^+\pi^-}}{16\pi}, \quad (48)$$

where Eq. 4 from Ref. [25] defines

$$\delta_B = \delta_B^{\pi\pi} + \delta_B^{K\bar{K}}. \quad (49)$$

Equation 28 from Ref. [25] is

$$\tan \delta_B^{K\bar{K}} = f_K(m) \cdot 2p_K = f_K(m) \cdot \sqrt{m^2 - 4m_K^2}, \quad (50)$$

where Eq. 36 from Ref. [25] gives

$$f_K(m) = -\arctan\left(\frac{m^2 - m_1^2}{m_2^2}\right) / \Lambda_K, \quad (51)$$

and we find the phase as

$$\delta_B^{K\bar{K}} = \arctan(\tan \delta_B^{K\bar{K}}). \quad (52)$$

The value of parameters m_1 , m_2 , and Λ_K used in our fits are listed in Table VIII.

5. *An exotic I=2 amplitude* $T_0^2(m) \equiv T_0^2(\pi^+\pi^+ \rightarrow \pi^+\pi^+, m)$

According to Ref. [17] the I=2 $\pi^+\pi^+ \rightarrow \pi^+\pi^+$ the rescattering amplitude is given in a unitarian form

$$T_0^2(m) \equiv T_0^2(\pi^+\pi^+ \rightarrow \pi^+\pi^+, m) = \frac{\eta_0^2(m) e^{2i\delta_0^2(m)} - 1}{2i}. \quad (53)$$

The phase shift $\delta_0^2(m)$ is parameterized by

$$\delta_0^2(m) = \frac{-a\sqrt{m^2/4 - m_\pi^2}}{1 + bm^2 + cm^4 + dm^6}. \quad (54)$$

From fit in Ref. [17] to data for the $\pi^-p \rightarrow \pi^0\pi^0n$ process in Refs [27] and [28], the parameters of Eq. 54 are $a = (55.21 \pm 3.18)$ deg/GeV, $b = (0.853 \pm 0.254)$ GeV⁻², $c = (-0.959 \pm 0.247)$ GeV⁻⁴, and $d = (0.314 \pm 0.070)$ GeV⁻⁶.

The $\eta_0^2(m)$ is an inelasticity for the wave with total spin 0 and isospin 2. In the mass range of $m < m(\rho\rho)$ (~ 1.54 GeV) the inelasticity parameter $\eta_0^2(m)$ should be represented by the smooth real function of m . An appropriate fit to data has been considered in Ref. [29], see their Fig. 2, and we use the approximation

$$\eta_0^2(m) = \begin{cases} 1, & m \leq 1 \text{ GeV}/c^2 \\ \propto \cos\text{-like smooth transition}, & 1 < m < 1.7 \text{ GeV}/c^2 \\ 0.4, & m \geq 1.7 \text{ GeV}/c^2. \end{cases} \quad (55)$$

In our case we neglect the small D wave scattering amplitude $T_2^2(\pi^+\pi^+ \rightarrow \pi^+\pi^+)$.

6. Mixing matrix $G_{RR'}(m)$

The mixing operator $G_{RR'}(m)$ is a matrix of inverse propagators, with rank equal to the number of mixed resonances. In case of mixing of two resonances R and R' this matrix has the form, following Eq. 5 of Ref. [25],

$$G_{RR'}(m) = \begin{pmatrix} D_R(m) & -\Pi_{RR'}(m) \\ -\Pi_{R'R}(m) & D_{R'}(m) \end{pmatrix}. \quad (56)$$

In general, the diagonal elements of this matrix are the inverse propagators

$$D_R(m) = m_R^2 - m^2 - im\Gamma_R(m), \quad (57)$$

while the non-diagonal elements are polarization operators describing mixing. An expression for the inverse propagator of the scalar resonance is given in Eq. 6 from Ref. [25],

$$D_R(m) = m_R^2 - m^2 + \sum_{ab} g_{Rab} [ReP_R^{ab}(m_R) - P_R^{ab}(m)], \quad (58)$$

where $\sum_{ab} g_{Rab} [ReP_R^{ab}(m_R) - P_R^{ab}(m)] = Re[\Pi_R(m_R)] - \Pi_R(m)$ takes in to account the finite width correction. After Eq. 5 in Ref. [25] the non-diagonal terms of the polarization operator are given by equation

$$\Pi_{RR'}(m) = \sum_{ab} g_{R'ab} P_R^{ab}(m) + C_{RR'}, \quad (59)$$

where the constants $C_{RR'}$ take into account effectively the contribution of VV , $4P$ and other intermediate states and incorporates the subtraction constants for the $R \rightarrow (PP) \rightarrow R'$ transitions. Here we use the notation from different publications, [22]–[25],

$$P_R^{ab}(m) = \frac{g_{Rab}}{16\pi^2} P^{ab}(m), \quad \text{or} \quad \Pi_R^{ab}(m) = \frac{g_{Rab}^2}{16\pi^2} P^{ab}(m), \quad (60)$$

and

$$\Pi_R(m) = \sum_{ab} \Pi_R^{ab}(m). \quad (61)$$

Eqs. 7–9 from Ref. [25] (also Ref. [23], Eq. 30 and Ref. [24], Eqs. 16,19,22) for $m_a > m_b$, $m_+ = m_a + m_b$, and $m_- = m_a - m_b$ give

$$P^{ab}(m) = \frac{m_+ m_-}{m^2} \ln \frac{m_b}{m_a} + \begin{cases} \rho_{ab}(m) \cdot \left[i\pi + \ln \frac{\sqrt{m^2 - m_-^2} - \sqrt{m^2 - m_+^2}}{\sqrt{m^2 - m_-^2} + \sqrt{m^2 - m_+^2}} \right], & m > m_+ \\ -\pi |\rho_{ab}(m)| + 2 |\rho_{ab}(m)| \arctan \frac{\sqrt{m_+^2 - m^2}}{\sqrt{m^2 - m_-^2}}, & m_- \leq m \leq m_+ \\ -\rho_{ab}(m) \cdot \ln \frac{\sqrt{m_+^2 - m^2} - \sqrt{m_-^2 - m^2}}{\sqrt{m_+^2 - m^2} + \sqrt{m_-^2 - m^2}}, & m < m_- \end{cases} \quad (62)$$

$$\rho_{ab}(m) = \sqrt{\left(1 - \frac{m_+^2}{m^2}\right) \left(1 - \frac{m_-^2}{m^2}\right)}. \quad (63)$$

The constants g_{Rab} are related to the width, Eq. 11 from Ref. [25],

$$\Gamma(R \rightarrow ab, m) = \frac{g_{Rab}^2}{16\pi m} \rho_{ab}(m). \quad (64)$$

7. Model parameters

In the mixing operator Eq. 56 we account for seven intermediate states: $\pi^+\pi^-$, $\pi^0\pi^0$, K^+K^- , $K^0\bar{K}^0$, $\eta\eta$, $\eta'\eta'$, and $\eta'\eta'$. We follow the conventions of Ref. [25] for coupling constants, motivated by the four-quark model. For the $f_0(980)$ and similarly for the σ we use

$$g_{f_0K^0\bar{K}^0} = g_{f_0K^+K^-}, \quad g_{R\pi^0\pi^0} = g_{R\pi^+\pi^-}/\sqrt{2}, \quad g_{R\pi\pi} = \sqrt{3/2}g_{R\pi^+\pi^-}. \quad (65)$$

For the $f_0(980)$ coupling constants to $\eta^{(\prime)}\eta^{(\prime)}$ we use

$$g_{f_0\eta\eta} = -g_{f_0\eta'\eta'} = \frac{2\sqrt{2}}{3}g_{f_0K^+K^-}, \quad g_{f_0\eta'\eta} = -\frac{\sqrt{2}}{3}g_{f_0K^+K^-}. \quad (66)$$

For the σ coupling constants to $\eta^{(\prime)}\eta^{(\prime)}$ we use

$$g_{\sigma\eta\eta} = g_{\sigma\eta'\eta'} = \frac{\sqrt{2}}{3}g_{\sigma\pi^+\pi^-}, \quad g_{\sigma\eta'\eta} = \frac{1}{3\sqrt{2}}g_{\sigma\pi^+\pi^-}. \quad (67)$$

Further we use the values of the parameters shown in Table VIII, which are taken from Fit 1 of Ref. [25].

TABLE VIII: Achasov model parameters from Fit 1 of Ref. [25] used in our calculations.

Parameter	Value in Fit 1 [25]	Parameter	Value in Fit 1 [25]
m_{f_0} , MeV	984.1	b_0	4.9
m_σ , MeV	461.9	b_1	1.1
$g_{f_0K^+K^-}$, GeV	4.3	b_2	1.36
$g_{f_0\pi^+\pi^-}$, GeV	-1.8	Λ , MeV	172.2
$g_{\sigma K^+K^-}$, GeV	0.55	m_1 , MeV	765.4
$g_{\sigma\pi^+\pi^-}$, GeV	2.4	m_2 , MeV	368.9
$C_{f_0\sigma}$	-0.047 [26]	Λ_K , GeV	1.24

8. Check for $\delta_{res}(m)$, $\delta_B^{\pi\pi}(m)$, $\delta_0^0(m)$, $\eta_0^0(m)$, etc.

In order to check that the code for this parameterization works properly we reproduce plots from Ref. [25].

$\delta_{res}(\mathbf{m})$: We define the $\delta_{res}(m)$ as the phase of the complex function $S_0^{0\ res}(m)$ in Eq. 42. However, this phase has discontinuities in the vicinity of each resonance mass, but not exactly at the resonance mass value. In further calculations we require that the phase is continuous, as shown in Fig. 22, by adding a phase shift of π above each discontinuity point. This plot is consistent with Fig. 3 in Ref. [25].

$\delta_B^{\pi\pi}(\mathbf{m})$: The background phase $\delta_B^{\pi\pi}(m)$ is derived from Eq. 44, as shown in Fig. 21. This plot is consistent with Fig. 2 in Ref. [25].

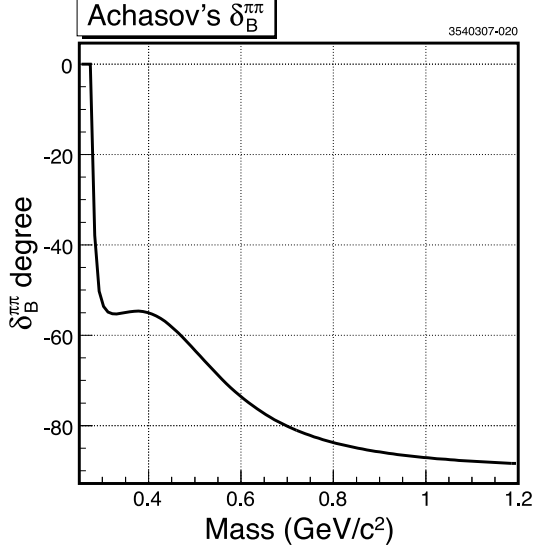


FIG. 21: The background phase in $\pi\pi$ scattering, $\delta_B^{\pi\pi}(m)$, from Eq. 44.

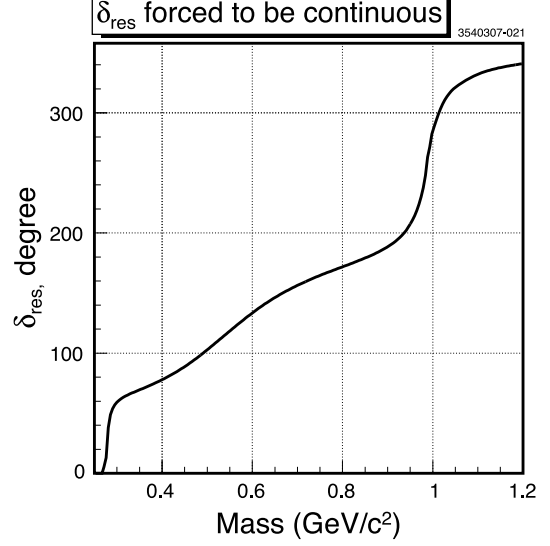


FIG. 22: The phase of the resonance $\pi\pi$ scattering, $\delta_{res}(m)$, from Eq. 42.

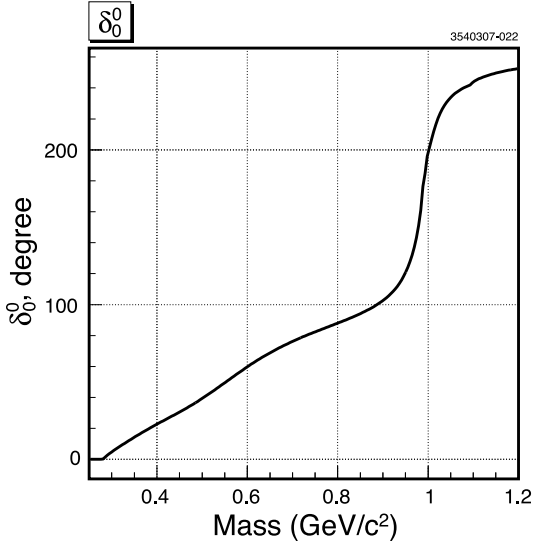


FIG. 23: The total $\pi\pi$ scattering phase, $\delta_0^0(m)$, from Eq. 39.

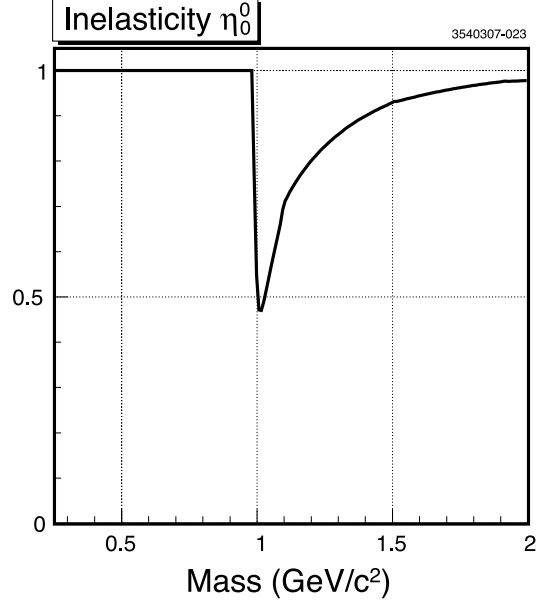


FIG. 24: The inelasticity, η_0^0 , from Eq. 41 for $2m_\pi < m < 2 \text{ GeV}/c^2$.

$\delta_0^0(\mathbf{m})$: The total phase $\delta_0^0(m)$ represented by Eq. 39 is shown in Fig. 23. This plot is consistent with Fig. 4 in Ref. [25].

$\eta_0^0(\mathbf{m})$: The $\eta_0^0(m)$ derived from Eq. 41 is displayed in Fig. 24 which shows that $\eta_0^0(m) = 1$ at $m < m_{K\bar{K}}$ confirming unitarity in $\pi\pi \rightarrow \pi\pi$ scattering, consistent with Fig. 6 from Ref. [25].

We also tested all complex functions and their components from Eq. 24. In particular, Fig. 25 shows $\delta_B^{K\bar{K}}$ from Eq. 52; Fig. 26 shows δ_B from Eq. 49; Figs. 27, 28 show the loop integrals $L_{K+K^-}(m|1,0)/16\pi$ and $L_{\pi+\pi^-}(m|1,0)/16\pi$, respectively, from Eq. 35.

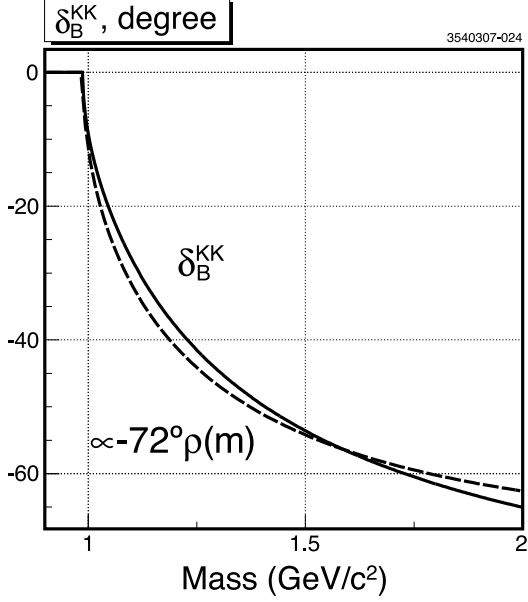


FIG. 25: The background phase in $K\bar{K}$ scattering, $\delta_B^{K\bar{K}}$, from Eq. 52 (solid curve), and its approximation by the phase space factor (dashed curve).

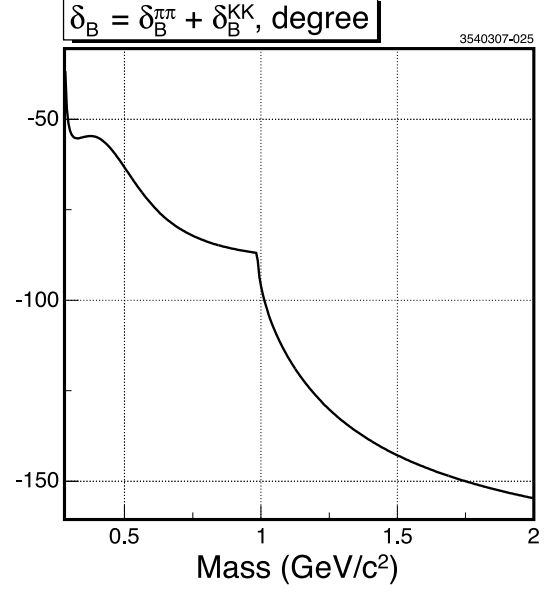


FIG. 26: The total background phase in $K\bar{K} \rightarrow \pi\pi$ scattering, $\delta_B = \delta_B^{\pi\pi} + \delta_B^{K\bar{K}}$, from Eq. 49.

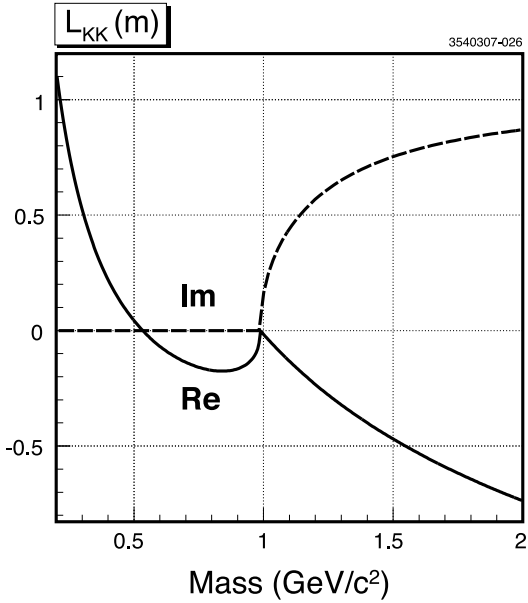


FIG. 27: The loop integral, $L_{K+K^-}(m, 1, 0)/16\pi$, from Eq. 35. The real (solid curve) and imaginary (dashed curve) parts of the complex function are shown.

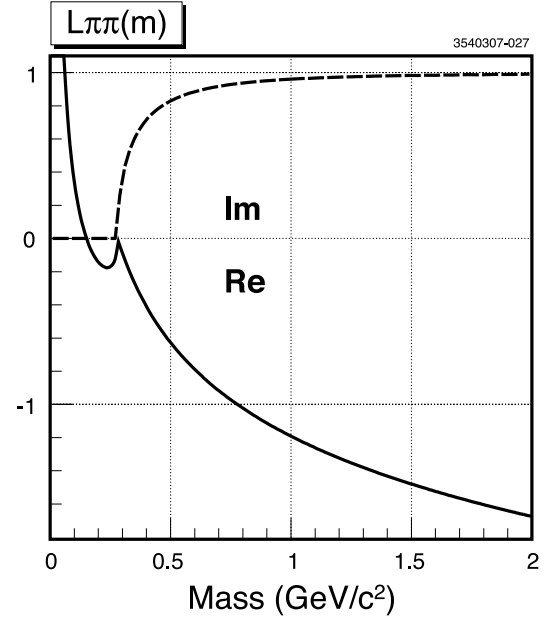


FIG. 28: The loop integral, $L_{\pi+\pi^-}(m, 1, 0)/16\pi$, from Eq. 35. The real (solid curve) and imaginary (dashed curve) parts of the complex function are shown.

9. S wave implementation in the code of the Dalitz plot fitter

As usually in a Dalitz plot analysis each amplitude fraction is taken with its own complex coefficient $c_{\text{mode}} = a_{\text{mode}}e^{i\phi_{\text{mode}}}$ represented by two real numbers, an amplitude a_{mode} and phase ϕ_{mode} . The loop integral in Eq. 35 has an additional offset constant d_{mode} . Unitarity requires that d_{mode} is real. All these constants, as well as unknown coupling constants $g_{D+\sigma\pi^+}$ and $g_{D+f_0\pi^+}$ from Eq. 45, are the fit parameters, which can be free to float or fixed. The actual parameterization for $m = m_x \equiv \min[m(\pi_1^+\pi^-), m(\pi_2^+\pi^-)]$ or $m = m_y \equiv \max[m(\pi_1^+\pi^-), m(\pi_2^+\pi^-)]$ is given by the amplitude

$$A_{\pi^+\pi^-}(m) = 16\pi c_{\pi\pi} \quad (68)$$

$$+ L_{\pi^+\pi^-}(m|c_{\pi\pi}, d_{\pi\pi}) \cdot \left(\frac{2}{3}T_0^0(m) + \frac{1}{3}T_0^2(m)\right) \quad (69)$$

$$+ L_{\pi^0\pi^0}(m|c_{\pi^0\pi^0}, d_{\pi^0\pi^0}) \cdot \left(\frac{2}{3}T_0^0(m) - \frac{2}{3}T_0^2(m)\right) \quad (70)$$

$$+ L_{K^+K^-}(m|c_{K^+K^-}, d_{K^+K^-}) \cdot T_0^0(K^+K^- \rightarrow \pi^+\pi^-, m) \quad (71)$$

$$+ L_{K^0\bar{K}^0}(m|c_{K^0\bar{K}^0}, d_{K^0\bar{K}^0}) \cdot T_0^0(K^0\bar{K}^0 \rightarrow \pi^+\pi^-, m) \quad (72)$$

$$+ c_{D+R\pi^+} \cdot T_0^0{}^{res}_{DR\pi}(m). \quad (73)$$

The I=2 $\pi^+\pi^+ \rightarrow \pi^+\pi^+$ scattering amplitude for $m = m_z \equiv m(\pi_1^+\pi_2^+)$ is given by

$$A_{\pi^+\pi^+}(m) = L_{\pi^+\pi^+}(m|c_{\pi\pi}, d_{\pi\pi}) \cdot T_0^2(m). \quad (74)$$

It is worth noting that three terms in Eqs. 68, 69 and 74 have a common complex coefficient $c_{\pi\pi}$, appearing from the point-like term, and two of them have a common offset parameter $d_{\pi\pi}$ from the loop integral. The total contribution of Achasov's S wave in the Dalitz plot amplitude is

$$A_{SW}(m_x, m_y, m_z) = A_{\pi^+\pi^-}(m_x) + A_{\pi^+\pi^-}(m_y) + A_{\pi^+\pi^+}(m_z). \quad (75)$$

The “ $DR\pi$ ” sub-mode in Eq. 73 has a redundant freedom for amplitude factors due to the products $a_{D+R\pi^+} \cdot g_{D+\sigma\pi^+}$ and $a_{D+R\pi^+} \cdot g_{D+f_0\pi^+}$. In our fits we fix $a_{D+R\pi^+} = 1$, or $a_{D+R\pi^+} = 0$ to turn it off, and use coupling constants $g_{D+\sigma\pi^+}$ and $g_{D+f_0\pi^+}$.

For a first approximation we try to eliminate the number of free parameters in the function. We assume $d_{\pi^0\pi^0} = d_{\pi\pi}$ and $d_{K^0\bar{K}^0} = d_{K^+K^-}$ from isospin symmetry. We note that the parameterization for $K^0\bar{K}^0 \rightarrow \pi^+\pi^-$ in Eq. 72 is nearly the same as that for $K^+K^- \rightarrow \pi^+\pi^-$ in Eq. 71. The small difference appears due to the different masses of the K^+ and K^0 mesons. Keeping in mind this small difference between amplitudes we do not consider separate contributions from $K^0\bar{K}^0 \rightarrow \pi^+\pi^-$ in this analysis. This means that the amplitude factor $a_{K\bar{K}}$ includes both contributions from $K^+K^- \rightarrow \pi^+\pi^-$ and $K^0\bar{K}^0 \rightarrow \pi^+\pi^-$.

The amplitude for $\pi^0\pi^0 \rightarrow \pi^+\pi^-$ in Eq. 70 has a different isospin factor at T_0^2 compared to the amplitude for $\pi^+\pi^- \rightarrow \pi^+\pi^-$ in Eq. 69 and different masses for π^0 and π^+ . In our fits we assume the equity $d_{\pi^0\pi^0} = d_{\pi\pi}$. The constant $c_{\pi\pi}$ also accounts for the point-like term in Eq. 68, and is involved in I=2 term, Eq. 74, that makes it different from the $c_{\pi^0\pi^0}$. For this reason we consider the $\pi^0\pi^0 \rightarrow \pi^+\pi^-$ sub-mode separately from $\pi^+\pi^- \rightarrow \pi^+\pi^-$.

[1] P.L. Frabetti *et al.* (E687 Collaboration), Phys. Lett. B **407**, 79 (1997).

- [2] J.C. Anjos *et al.* (E691 Collaboration), Phys. Rev. Lett. **62**, 125 (1989).
- [3] E.M. Aitala *et al.* (E791 Collaboration), Phys. Rev. Lett. **86**, 770 (2001).
- [4] J.M. Link *et al.* (FOCUS Collaboration), Phys. Lett. B **585**, 200 (2004).
- [5] R.H. Dalitz, Philos. Mag. **44**, 1068 (1953).
- [6] J.A. Oller, Phys. Rev. D **71**, 054030 (2005).
- [7] D.V. Bugg, Phys. Lett. B **632**, 471 (2006).
- [8] S.M. Flatté, CERN/EP/PHYS 76-8, 15 April 1976; Phys. Lett. B. **63**, 224 (1976).
- [9] J. Schechter, Int.J.Mod.Phys. **A20**, 6149 (2005).
- [10] Private communication with N.N. Achasov, 2005-2006. See References [17], [21]-[25].
- [11] G. Viehhauser, Nucl. Instrum. Methods A **462**, 146 (2001); D. Peterson *et al.*, Nucl. Instrum. Methods Phys. Res., Sect. A **478**, 142 (2002); Y. Kubota *et al.*, Nucl. Instrum. Methods Phys. Res., Sect. A **320**, 66 (1992); R.A. Briere *et al.* (CESR-c and CLEO-c Taskforces, CLEO-c Collaboration), Cornell University, LEPP Report No. CLNS 01/1742 (2001) (unpublished).
- [12] G.S. Huang *et al.* (CLEO Collaboration), Phys. Rev. Lett. **95**, 181801 (2005); T.E. Coan *et al.* (CLEO Collaboration), Phys. Rev. Lett. **95**, 181802 (2005).
- [13] P. Rubin *et al.* (CLEO Collaboration), Phys. Rev. Lett. **96**, 081802 (2006).
- [14] S. Kopp *et al.* (CLEO Collaboration), Phys. Rev. D **63**, 092001 (2001).
- [15] J.M. Blatt and V.F. Weisskopf, *Theoretical Nuclear Physics*, Wiley, New York, 1951, p.361.
- [16] W.-M. Yao *et al.*, Journal of Physics G **33**, 1 (2006).
- [17] N.N. Achasov and G.N. Shestakov, Phys. Rev. D **67**, 114018 (2003).
- [18] M. Ablikim *et al.* (BES Collaboration), Phys. Lett. B **607**, 243 (2005).
- [19] D. Black, A.H. Fariborz, S. Moussa, S. Nasri, J. Schechter, Phys. Rev. D **64**, 014031 (2001).
- [20] M. Gell-Mann and M. Levy, Nuovo Cimento **16**, 705 (1960).
- [21] N.N. Achasov, S.A. Devyanin, G.N. Shestakov, Yad. Fiz. **32**, 1098 (1980) [Sov. J. Nucl. Phys. **32**, 566 (1980)].
- [22] N.N. Achasov and A.A. Kozhevnikov, Phys. Rev. D **55**, 2663 (1997).
- [23] N.N. Achasov and V.V. Gubin, Phys. Rev. D **56**, 4084 (1997); Yad. Fiz. **61**, 274 (1998) [Phys. Atom. Nucl. D **61**, 224 (1998)].
- [24] N.N. Achasov and A.V. Kiselev, Phys. Rev. D **70**, 111901(R) (2004).
- [25] N.N. Achasov and A.V. Kiselev, Phys. Rev. D **73**, 054029 (2006).
- [26] The constant $C_{f_0\sigma}$ has an opposite sign comparing to Ref. [25] (N.N. Achasov, private communication, typo in Ref. [25]).
- [27] W. Hoogland *et al.*, Nucl. Phys. B **126**, 109 (1977).
- [28] N.B. Durusoy *et al.*, Phys. Lett. **45B**, 517 (1973).
- [29] B.S. Zou *et al.*, published in Hadron 03 Proceedings, AIP Conf.Proc.717:347 (2004).